www.sciencemag.org/content/356/6335/311/suppl/DC1

Supplementary Materials for

Biased partitioning of the multidrug efflux pump AcrAB-TolC underlies long-lived phenotypic heterogeneity

Tobias Bergmiller,* Anna M. C. Andersson,* Kathrin Tomasek, Enrique Balleza, Daniel J. Kiviet, Robert Hauschild, Gašper Tkačik, Călin C. Guet†

*These authors contributed equally to this work.
†Corresponding author: calin@ist.ac.at

Published 21 April 2017, *Science* **356**, 311 (2017)
DOI: 10.1126/science.aaf4762

This PDF file includes:

Other Supplementary Material for this manuscript includes the following:
(available at www.sciencemag.org/cgi/content/full/356/6335/311/DC1

Materials and Methods

Media and chemicals

Two different types of growth medium were used throughout the study. First, all strains were maintained and grown in Luria Broth (LB) media (Lennox, Sigma) for standard genetic techniques and grown on LB agar plates (1.5% agar, Sigma). Second, all microfluidic experiments and the required bacterial pre-cultures were grown in M9-based defined rich medium, which consisted of 1xM9 salts, 1x casamino acid hydrolysate, 0.2% glucose, 1mM $MgSO_4$, 0.1mM $CaCl_2$ and 0.01% Tween 20 (all Sigma). We will refer to this media as microfluidics media throughout the manuscript. The constituents were autoclaved separately, and mixed and diluted to the indicated concentrations with sterile Millipore water. The addition of low amounts of a mild detergent such as Tween or Triton prevents excessive attachment of bacterial cells to polydimethylsiloxan (PDMS) or glass surfaces, and is commonly used in microfluidic systems (*26*). Antibiotics (ampicillin, chloramphenicol, tetracycline, doxycycline, erythromycin, kanamycin) were from Sigma, as were the inducers isopropyl-β-D-thiogalactopyranoside (IPTG) and L-arabinose. In detail, the antibiotics used for MIC measurements and microfluidic experiments were chloramphenicol (Sigma #C0378), tetracycline (Sigma #87128), doxycycline hyclate (Sigma #D9891), erythromycin (Sigma #E5389), and kanamycin sulfate (Sigma #60615). Buffer substances used for immunofluorescence experiments (PBS, TRIS-HCl, EDTA, lysozyme, bovine serum albumin (BSA)) and Hoechst 33342 (H33342) were from Sigma.

Strains and growth conditions

All strains used for experiments were derivatives of MG1655 or BW27784 as indicated, while all cloning was done using DH5α or its pir+ strain variant. Lambda red recombineering was done in strain DY330 or using the plasmid pSIM6 (a gift from Donald Court, National Cancer Institute, Frederick, MD 21702, USA) following previously described protocols (*27*). Recombineering into DY330 was followed by general P1 transduction of the engineered site into MG1655. Single-copy insertion of plasmids with R6K origins of replication (CRIM plasmids) was done as described elsewhere (*28*). MG1655 and DH5α/DH5α pir+ were grown at 37°C, DY330 and strains harboring the plasmids pSIM6, pCP20 (*29*), pINTts or pAH121 (*28*) were grown at 30°. Liquid cultures were grown in 37°C or 30°C with 250rpm in 14ml loose-cap plastic tubes (Falcon), and derived by diluting overnight cultures 1:1000. Overnight cultures were started from a single *E. coli* colony from a fresh streak on LB agar plates. Strains were cryo-preserved at -80°C as glycerol stocks (12% glycerol) made from overnight cultures.

Strain construction

We used the template plasmid pKD3-msfGFP (lab strain collection; msfGFP containing monomeric A206K mutation, from Addgene; msfGFP is abbreviated as GFP throughout the main text) to generate PCR products using Phusion polymerase (NEB) that would fuse the coding sequences of fluorescent proteins in-frame to the 3'-ends of *acrB* or *tolC* by lambda red-mediated recombineering. To do so, the 5' oligonucleotides were designed to remove the stop codon of the desired target gene, followed by a nine amino acid long hydrophilic, codon-optimized and disordered polylinker (GSGNKGQG)

and the fluorescent protein coding sequences lacking their start codons. The 3' oligonucleotides removed 20 nucleotides from the downstream region of *acrB* and *tolC*. Purified PCR products were electroporated into lambda-red competent cells, and integrants were selected for with 15μg/ml chloramphenicol. Selected clones were tested for insertions by colony-PCR, and the insertion including the junction between the chromosomal genes and the fluorescent protein coding sequence was sequenced. In a second step, the adjacent chloramphenicol marker was removed using pCP20. The functionality of all protein fusion carrying strains was assessed by measuring their susceptibility to tetracycline in serial dilution tests (see **Figure S2 and Table S8**).

For pulse-chase experiments, *acrAB-gfp* and, as a control for functionality native *acrAB*, were modified by introduction of the arabinose-inducible P_{araBAD} promoter. The detailed method of construction was described previously (*30*). Briefly, 5' and 3' homology regions were chosen to remove the endogenous *acrAB* promoter and the adjacent *acrR* gene, and the promoter junction to *acrAB* was PCR-verified. The constructs were then moved by P1 transduction into the strain BW27784, which allows for linear induction with L-arabinose (*31*). The functionality of the resulting strains was assayed by measuring arabinose-dependent sensitivity towards tetracycline. P_{araBAD} driving cytoplasmic GFP (P_{araBAD}-*gfp*) was encoded on a low-copy plasmid (*32*).

To achieve mild levels of *tolC* expression and complementation of *tolC* deletion, we cloned the open reading frame of *tolC* into pAH55 behind a P_{tac} promoter (*28*) using NdeI and SalI, followed by insertion into *attλ* with pINTts and single-copy insertion verification by PCR. Addition of 200μM IPTG led to wild type levels of tetracycline sensitivity in an *acrB-gfp* Δ*tolC* strain (**Figure S7**).

Chromosomally encoded and constitutively expressed mCherry fluorescent protein driven by the right lambda promoter (PR) was constructed by inserting pAH81-PR-*mCherry*::*FRT-chlor* (lab strain collection) into the phage 21 attachment site (*attP21*) using the helper plasmid pAH121. We did not observe growth reduction or detrimental effects of strains carrying single-copy PR-*mCherry* at *attP21*. If needed, the inserted PR-*mCherry* construct was moved into other strain backgrounds using transduction with P1 phage, selecting for transductants with 15μg/ml chloramphenicol.

To detect the localization of AcrB using immunofluorescent labeling with an antibody, we constructed a chromosomally encoded triple flag-tag (3xFlag; DYKDHDGDYKDHDIDYKDDDDK) variant of AcrB using pSUB11 (a gift from Lionello Bossi, CNRS, 91198 Gif-sur-Yvette, France) and lambda red recombineering. The 5' primers were designed to remove the stop codon of the target gene, and to fuse a short stretch of nucleotides encoding the 3xFlag in-frame to *acrB*. Recombineering was done as described, except that integrants were selected using 50μg/ml kanamycin. Integrants were verified by colony PCR and the junctions were sequenced.

Microfluidics master fabrication

Fabrication of the template for the microfluidic device was carried out using standard soft lithography techniques at the FIRST cleanroom facility at ETH Zurich. We created a 2D design for the flowcell using TannerTools L-Edit software. The design consisted of 8 parallel flow channels with a length of 20mm and a width of 200μm, splitting into two 100μm wide channels in the middle. Perpendicular to the middle of the

flow channels, every 5μm a 24μm long growth channel was placed. The width of these growth channels ranged from 1.2μm to 1.6μm. Chrome-layered photomasks of the design were obtained from Compugraphics Jena, Germany. In the first photolithography step the growth channels were deposited on a clean 4 inches silicon wafer. 3mL of SU8-2000.5 (MicroChem) was spun onto the wafer for 30s at 3000rpm, after which it was UV-exposed in a Karl Süss MA6 mask aligner using vacuum contact and a total power of 48mJ/cm^2. The exposed wafer was developed using mrDev 600 (micro resist technology). The second photolithography step consisted of depositing the flow channels on top of the growth channels. SU8-3025 (MicroChem) was spun onto the wafer for 30s at 3000rpm. After alignment of the wafer to the mask, it was UV-exposed with a total power of 160mJ/cm^2 and developed using mrDev 600. Feature dimensions were verified by profilometry and consisted of approximately 1.1μm high growth channels and 30μm high flow channels. Final width of growth channels was approximately 1.2μm to 1.6μm, and the length of growth channels was between 24μm and 25μm.

Microfluidic device construction

The wafers were glued on to glass petri dishes. 25ml of PMDS was mixed 1:10 with curing agent by vigorous stirring, then poured onto the wafer, and degased in a desiccator under vacuum until all air bubbles disappeared. Then, the PDMS was cured at 75°C overnight. The next day, the PDMS was cut out around the wafer, and further cut to a size of 45mm x 20mm. Holes for inlets and outlets were punched using a sharpened 22ga luer stub (from Instech). Before bonding, the surface of the imprinted features was cleaned using scotch tape, and the glass cover slip (24mm x 50mm, thickness 0.17mm+/-0.005, from Carl Roth) was extensively washed with ethanol. Then, the cover slip and PDMS with the features upwards were exposed to air plasma in vacuum for 60s, and the activated PDMS was put on top of the activated site of the glass cover slip. The bonded device was incubated for 1h on a heating plate at 80°C to strengthen the bonding.

Culturing of *E. coli* in mother machine devices

Before loading bacterial cells, the device was loaded with microfluidics media. To inject media, a 22ga luer pin was connected to a few centimeters of BPE-T50 tubing (Instech) and connected to a filled 5ml syringe using a 22ga luer stub. The preloaded device was incubated for 1hr to allow media to fill all channels. Then, the device was loaded with bacteria as follows: bacterial cultures were started 1:1000 from overnight cultures and grown to an OD of 0.25 to 0.5. Cultures were concentrated 1:50 to 1:80 fold by pelleting and resuspending cells in fresh media. To load cells into the device, 15μl of culture were injected using a pipette.

We subjected strains to the experimental conditions simultaneously by co-culturing these strains in mother machine devices, when applicable. Up to three different strains that could be separated by the properties of the expressed fluorescent protein fusions and constitutive fluorophores were mixed and injected into the same device. To allow cells to settle into the growth chambers, the loaded device was incubated at room temperature for 30min, and another 30min on the microscope stage of the preheated microscope at 30°C. At that point, the device was fixed to a custom-made aluminum holder with a drop of cyanoacrylate-based glue to prevent any movement of the device during imaging. This procedure did not alter growth rate, nor did it lead to stationary phase. Addition of fresh

medium led to immediate regrowth of cells such that within two to three generations exponential growth rate was achieved. All microcopy experiments were run at 30°C.

For microfluidic operation we used 60ml syringes (BD) as reservoirs for microfluidics media operated by syringe pumps (NE-1000). Tubing was connected to syringes using male luer connectors (Carl Roth, CT58.1) that fit tubing with an inner diameter of 1.27mm (Tygon S-54HL, 2.286 outer diameter). Smaller tubing connecting to the device with 22ga luer pins was connected to larger tubing using luer stubs and male luer connectors. Tubing was connected to the device with an initial flow rate of 4ml/h for 5min to push out excess cells. The flow was reduced afterwards to 2ml/h and kept constant throughout the whole experiment.

To mix temporal gradients of tetracycline, tubing of two syringe pumps was connected using a y-connector. Directly after the y-connector, the tubing was reduced to an inner diameter of 0.58mm. The tubing dimensions in between mixing experiments were kept constant to allow for reproducible results. To mix the flow of two pumps we reduced the flow rate of one pump and increased the flow rate of the other pump while keeping the total flow rate of 2ml/h constant. Syringe pumps were controlled by custom-made software (LabView). To test the mixing efficiency of the system, we calibrated the system by mixing fluorescein in a stepwise fashion analogous to the drug mixing experiments.

Single-cell efflux assays

Single-cell efflux profiles were measured of cells cultured for approximately 900min inside mother machine devices by switching to microfluidics media containing 5μM Hoechst33342 (H33342). H33342 is membrane permeable, and is a substrate for AcrB and AcrF, and is TolC-dependent (*17*). After entering the cell, H33342 binds to the minor groove of DNA, upon which it becomes excitable by 390nm light. Thus, efflux activity is inversely correlated with the amount of H33342 bound to the bacterial chromosome, and active dye efflux by AcrAB-TolC determines dye levels inside bacterial cells. After addition of H33342, cells were imaged using illumination setting for DAPI.

Microscopy

Microscopy was done using an inverted Nikon Ti-Eclipse microscope with a perfect focus system, an automated stage and shutters, enclosed in a custom-made incubation box connected to a temperature controller from Reinach (Life Imaging Services, Switzerland). Multiple positions of up to three parallel microfluidic devices were imaged during one experiment, and fluorescence images were acquired every 6min if not indicated differently. All images were taken using a 100x 1.4 NA oil immersion objective lens. A Lumencore LED unit with a neutral density filter factor 8 in the light path was the light source for all experiments, and the light intensity of all used LEDs was monitored regularly. To image constitutive mCherry, the green LED (549+/-15nm) was used at a light intensity of 320μW and an exposure time of 300ms. To image AcrB-GFP and TolC-GFP, the cyan LED (475+/-28nm) at a light intensity of 230μW and an exposure time of 250ms was used. To image H33342, we used the violet LED (390+/-18nm) with an exposure time of 200ms and a light intensity of 150μW. The emission filters were from Chroma with the following specifications: DAPI LP 409, BP447/60; GFP LP 495 BP

520/35; TexasRed HYQ LP 596, BP 641/75. A water-cooled CCD Hamamatsu Orca-R2 camera with a pixel size of 0.0645 microns/pixel with gain set to 200, or a cooled Hamamatsu EMCCD C9100-02 pixel size 0.08 microns/pixel with EM-gain set to 170 was used, with a 0.7 c-mount adapter installed between camera and microscope. Images were acquired with NIS-Elements.

Total internal reflection fluorescence microscopy

For TIRF microscopy, strains expressing chromosomally encoded AcrB-GFP or TolC-GFP, in strain backgrounds as indicated, were grown to OD_{600nm}=0.1 in microfluidic growth medium, which contained 0.05% casamino acids to reduce background autofluorescence. Agarose pads were prepared by casting agarose molten in low-autofluorescence medium between two glass slides spaced by two cover slips. A 2x2mm square was cut out, placed onto a glass slide, and 1ml of bacterial culture was spotted onto it and allowed to dry. The pad was framed by a double-sided sticky 9x9mm frame seal (Bio-Rad SLF0201) and covered with a high-precision and clean room grade cover slip (Schott Nexterion glass D, thickness 0.170+/- 0.005mm). Imaging was done at 30°C with a temperature-controlled Olympus IX83 total internal reflection fluorescence microscope equipped with a water-cooled Hamamatsu ImageEM C9100-13 camera, a 100x 1.49NA objective lens and an additional 2x magnification tubular lens giving an effective pixel size of 80nm/pixel. Images were acquired every 20s using a single-band pass GFP filter and a diode 488nm laser set to an output of 0.4mW and low camera gain settings. AcrB-GFP was imaged at 75nm penetration depth, and TolC-GFP at 65nm penetration depth. Images were corrected, if necessary, for motion using the ImageJ "StagReg" plugin. Kymographs of elongating cells were created using the ImageJ plugin "MultiKymograph" by drawing a segmented line of thickness 3 through cells at the end of the cell cycle. For two-generation kymographs, separate kymographs of cells before and after cell division were made and assembled. Before kymographs were created, a mean filter of pixel size 1 was applied to images.

Immunofluorescence

The protocol to immunolabel *E.coli* cells inside microfluidic mother machine devices was adapted from (*33*). In detail, a 3-way switch was build into the inflow tubing, and all alternating buffer conditions were applied by careful manual injection using 5ml syringes. After 14h growth inside the microfluidics device, cells were fixed for 20min by manually injecting 2ml of 2% formaldehyde in PBS solution, followed by washing the device with 2ml cold PBS. Then, 2.5ml permeabilizing buffer (50mM Tris-HCl pH8, 5mM EDTA pH8, 2.5ug/ml lysozyme) was applied and incubated for 10min, followed by a wash step using 2.5ml PBST (PBS with 0.05% Tween 20). 2.5ml PBST with 1%BSA (blocking buffer) was added, and incubated for 30min. In the next step, primary Anti-Flag Alexa488 antibodies (from Cellsignal, item number 5407) were diluted 1:500 in 2ml blocking buffer, applied to the device and incubated for 30min. In the last step, the device was washed twice with 2ml PBST with a 10min incubation time between the washes. Alexa488 labeled proteins were imaged, and 23 Z-stacks with 250nm step size were recorded. To test for labeling specificity, cell expressing a constitutive mCherry only were mixed with mCherry and an AcrB-3xFT-expressing strain. Because the first cell that enters a growth channel and starts dividing determines which strain grows inside this

channel, the channels are occupied by isogenic cells of one specific strain only. Thus, partial labeling of cells in individual channel is an indication for unspecific labeling. We found that either all cells or none of the cells inside specific growth channels were labeled, which indicated highly specific labeling (**Figure S6**).

Fluorescence-activated cell sorting (FACS)

Strains expressing AcrB-GFP, AcrB-GFP in a Δ*tolC* background, and as a control strain expressing a plasmid-based GFP were used for FACS sorting. All strains expressed chromosomally encoded and constitutively expressed mCherry. Cultures were grown overnight in 0.2μm filtered microfluidics media without Tween20 at 30°C. Fresh 1 to 1000 dilution cultures were grown in medium for 4h at 30°C to early exponential phase.

Cells were sorted using FACS AriaIII flow cytometer (BD Biosciences, San Jose, CA). The 70 micron sort setup was used for droplet formation. For sorting, the sample temperature was set to 4°C and sorted cells were kept on ice until further assessment. Sensitivity of the lasers was determined within the daily setup using BD FACS 7-color setup beads and the delay in droplet formation was determined for optimal sorting using the BD FACS Accudrop technology. A 488nm laser with 20mW used for scatter and fluorescence detection. The forward scatter (FSC) detector was a photodiode with a sensitivity of 0.5 micron and with voltage set to 566. In front of the FSC detector a 1.0 neutral density filter was installed. The side scatter (SSC) detector was a photomultiplier tube with a sensitivity of 0.5 micron and with voltage set to 374. Both signals were collected through a 488/10nm band-pass filter. The fluorescence detector was a photomultiplier tube with voltage set to 703, and green emission from FITC-A was collected through a 530/30nm band-pass filter. A 561nm green laser with 50mW was used for mCherry fluorescence detection. The mCherry fluorescence detector was a 610/20nm band-pass filter with voltage set to 900. Particle counts were plotted on log scale with thresholding on FSC and SSC at 1,000.

The fluorescence signal from the bacterial population, gated on FSC and mCherry fluorescence, was biexponentially transformed. We found that sorting any GFP signal on FSC and SSC yielded two subpopulations that differed in efflux activity, and we assumed that the gating procedure biased sampled cells to small cells (left tail, low GFP fluorescence) and large cells (right tail, high GFP fluorescence). Thus, we gated populations on FSC, which is a proxy for cell size, and chromosomally encoded constitutively expressed mCherry as a proxy for viability. For sorting, bacterial cultures were diluted into ice-cold medium to achieve approximately 10.000 events/s at a flow rate of 1.0 – 1.4. Directly before sorting, 20.000 events were recorded and a gate including 98% of all events gated on the constitutive mCherry-A signal and the FSC-A signal was drawn using the FACSDiva software. From this population the FITC-A histogram was displayed and the highest 10% quantile (right tail) and the lowest 10% quantile (left tail) of the distribution were gated. 1,000,000 events of each quantile were sorted at an efficiency of above 80% into 500μl cooled medium using the 70 micron nozzle for droplet formation and 1x PBS as sheath fluid. FACS data were analyzed using FACSDiva software (version 6.1.3, BD Biosciences) and FlowJo software (version 10.0.7, FlowJo LLC).

Mean AcrB-GFP fluorescence of AcrB-GFP and AcrB-GFP Δ*tolC* strains as proxy for gene expression was measured with a FACS Canto analyzer. Mean fluorescence

levels were determined using FlowJo (version 10.0.7, FlowJo LLC) from three independent cultures and 20.000 events each, after gating on 5000 events on SCC and FSC.

Fluorescence efflux assay on FACS sorted populations

The 96-well plate fluorescence assay for assessment of active efflux by (*17*) was adapted to analyze the differences in efflux activity between sorted *E. coli* populations – one population with high levels of AcrB-GFP (highest 10% quantile) and one population with low levels of AcrB-GFP (lowest 10% quantile). As efflux control, a single-gene deletion mutant missing the outer membrane part of the multidrug efflux pump, TolC, while expressing AcrB-GFP, was subjected to the same sorting and efflux protocol. To test whether sorting of the right and left tails of any GFP signal would yield populations that differ in efflux activity, we sorted a reference strain constitutively expressing GFP (GFP expressed from pZS*1R-GFP, lab strain collection), and subjected the populations to the same efflux assay.

Sorted bacterial cells were spun down at 4,000 rpm for 10min at 4°C and resuspended in 1 ml cold 1x M9 salts (5x M9 salts: 2.5 g/l NaCl, 5 g/l NH_4Cl, 33.9 g/l Na_2HPO_4, 15 g/l KH_2PO_4) supplemented with 1mM $MgSO_4$ and 0.1mM $CaCl_2$. Prior to the efflux assay a small aliquot from each sorted subpopulation was taken to estimate recovery of the sort by plating 5µl spots of serial dilutions using 1x M9 salts supplemented with Mg^{2+} and Ca^{2+} on LB agar plates. Colony forming units (CFUs/ml) were calculated after overnight incubation at 30°C from the lowest countable dilution.

180µl aliquots of sorted bacterial populations were transferred to a 96-well plate (clear flat-bottom, black, Corning Incorporated, Costar, NY) and 5 replicates per sorted population were measured. 20µl of Hoechst 33342 (H33342; Sigma-Aldrich) was added to a final concentration of 10µM using a Synergy H1 microplate reader with injectors (BioTek Instruments, VT) and Gen5 software (version 2.01.13, BioTek Instruments). The monochromators for optical detection were set to excitation 355nm, emission 460nm and a gain multiplier of 90. After dispensing H33342, the plate was mixed at slow orbital speed at 180rpm for 5s. Fluorescence was recorded from the top of the wells for 30 cycles measuring every 75s at 30°C. Five data points per well per read were recorded, and the mean of each well was calculated as the mean relative fluorescence units (mRFUs) using the Gen5 software. These values were exported and used for further calculation using Excel. All data were normalized by M9 as blank and the amount of cells calculated as CFU/ml.

Determining P_{tac} induction

A strain harboring a single-copy insertion of pAH55-P_{tac}-*mVenus* in the lambda attachment site was inoculated 1:200 from overnight culture into a 96well plate (clear flat-bottom, black, Corning Incorporated, Costar, NY) prefilled with 200µl microfluidic growth medium supplemented with different IPTG concentrations. Bacterial growth and fluorescence was measured in a Synergy H1 microplate reader (BioTek Instruments, VT) set to 30°C at continuous double-orbital shaking with a sampling rate of 4min. Optical density was measured at 600nm, and mVenus fluorescence was detected at 545nm with excitation at 515nm and detector gain set to 100. P_{tac}-mVenus expression levels were determined by subtracting the cellular autofluorescence of a non-fluorescent MG1655

wildtype strain from the mVenus expressing strain ($Fluorescence_{mVenus}/OD_{mVenus}$ - $Fluorescence_{wt}/OD_{wt}$) over a whole growth curve. mVenus becomes detectable at around 4.5h in late exponential phase, after which the fluorescent signal continuously increases due to fluorophore accumulation.

Image processing

All image processing was done using the freeware FIJI, and brightness and contrast were adjusted linearly. Files were split into XY positions and different fluorescence channels, and cropped, rotated and corrected for motion using ImageJ, if required, before tracking with a custom-made Matlab script.

Image segmentation

We used an in-house built cell segmentation and lineage tracking algorithm that was customized for mother-machine data. Briefly, edge detection is performed on the complete image of each channel in a microfluidic device. Based on the detected edges, the full image is divided into sub-images containing one cell each. A cell segmentation mask is constructed from the fluorescence channel in which we image constitutive expression of cytosolic protein (mCherry for AcrB-GFP and TolC-GFP fusions and for the reference strain without protein fusions). The segmentation threshold is estimated using Otsu's method (MATLAB graythresh) and conservatively increased by 20%; segmentation mask is then extracted using MATLAB im2bw function. The mask is cleaned up by removing any specks smaller than 0.5 μm^2. The mask is rejected if it consists of more than 3 disjoint components; if it contains 2 or 3, it is manually inspected to see which combination of components corresponds to an individual cell. A tracked cell is added to the dataset if its segmentation mask is not rejected in any of the frames, which results in 0.5-2% of all cells being discarded in the experiments for Figure 1 and 2 and 2-3% in the experiments with antibiotics in Figure 3. Cells in a channel can be lined up at a small angle and can thus protrude into neighboring cells' sub-images, rather than belonging to fully disjoint sub-images with no overlap. The final step of segmentation consists of resolving these 'overlap regions' by assigning their pixels to identified cells whose masks are geometrically the closest.

Sampling rate

We measured fluorescence (both in the constitutive and protein fusion channels, and the dye (DAPI) channel in the dye experiment) as well as cell geometry derived from the segmentation mask (e.g., cell length) at every frame. Default interval between frames is 6 min; for the dye efflux experiments, it is 1.5 min; and for the pulse chase experiment it is 4 min. For certain measurements we only report values at frames just before and just after cell divisions, as specified in the main text.

Cell growth and size

Cell length is calculated from the segmentation mask, by finding extremal coordinates of the mask in each dimension and computing length as

$$l = \sqrt{(y_{max} - y_{min})^2 + (x_{max} - x_{min})^2}.$$

Elongation rate α is extracted assuming exponential growth: it is calculated separately for each cell cycle as a slope of the best-fit line to the *log l(t)* as a function of *t*.

The number of points over which the exponential is fitted is equal to the cell cycle duration measured in frame interval units; typical values are 5 frames for no antibiotic condition, and for conditions II, III, IV, V (see main text) the corresponding values are 7, 13, 19, 19 frames. Cell cycle duration T is the number of frames between two identified division events multiplied by the frame interval; T is thus reported in integer multiples and its resolution is limited by the imaging interval.

Fluorescence measurements

Background fluorescence is estimated in every channel separately from two cell-free rectangular areas ('background areas') each spanning 10% of the width of the sub-image, aligned at the sides of the cell parallel to its long axis and to the microfluidic channel. The pixel intensity values in all sub-images are additively shifted so that the average background fluorescence estimated in every sub-image is equal; we find that this procedure normalizes for slow temporal and positional fluctuations in overall image intensity. To construct the mask for the extraction of fusion protein fluorescence, we use the segmentation mask from the constitutive channel, find its maximal linear extent parallel to the microfluidic channel, and compute its midpoint. The midpoint together with the extremal points of the mask defines the extent of the two cell-halves. We then define two rectangular cell-half masks aligned with the microfluidic channel that extend 10 pixels (0.65μm) beyond the extremal points of the segmentation mask. This is because AcrAB-TolC efflux pumps are located in the cell envelope and their fluorescence can often be found slightly beyond the confines of the segmentation mask itself. The pump fusion fluorescence in cell-halves is estimated from these rectangular masks. To compute various statistics of the fluorescent signal in pixels belonging to cell-half masks, we first take the histogram of pixel intensity values in the cell-half masks at every frame and subtract from it the histogram expected due to background, estimated from the corresponding background areas.

All fluorescence measurements in the fusion and dye channels are computed from cell-half measurements. Whole cell mean fluorescence is the average over the two cell-half measurements. Total cell fluorescence is the whole cell mean fluorescence multiplied by the cell length.

In the H33342 dye experiments the dye also has some affinity for the microfluidic chip material, making the above procedure for estimating the background unreliable; additionally, the dye signal exhibits its own spatio-temporal kinetics as it diffuses into the microfluidic channels. To take these effects into account, we constructed average background kymographs from the dye fluorescence in empty channels (Multi Kymograph plugin in ImageJ), align it in space and time to images of full channels and subtract it from each full channel image. Measuring fluorescence of the DNA binding dye is done in an area which is bounded by the segmentation mask for each half of the cell.

Model

To gain insight into population level effects expected from biased sampling we developed a stochastic model that contains three processes contributing to the total protein count in a cell: production, partitioning, and inheritance. We assumed that the protein production is a Poisson process with rate 2λ, and that proteins made in the current cell cycle (generation) partition binomially with no bias, $q = 0.5$, between the sister cells.

In contrast, proteins inherited from previous generations undergo a biased binomial partitioning, with $q \neq 0.5$. Binomial sampling from a Poisson distribution yields a Poisson distribution with an average that depends on the probability of sampling. As a result, after division (in generation $g+1$) the newly produced protein will be distributed according to *Poisson(*λ), while the inherited protein will be distributed according to *Poisson(*μ_{gi}*),* where μ_{gi} is the average number of proteins in the i-th cell of the generation g; this quantity is different between cells. The full distribution of protein amounts in generation $g+1$ will be a convolution between these two distributions. We calculated the distribution of proteins U in each cell after g generations, by a probability generating function for the new proteins U_N and the inherited proteins U_D.

$$P(U_N = u_N) = \frac{\lambda^{u_N}}{u_N!}\, e^{-\lambda} \Longrightarrow g_{u_N}(z) = e^{\lambda(z-1)}$$

$$P(U_D = u_D) = \frac{{\mu_{gi}}^{u_D}}{u_D!}\, e^{-\mu_{gi}} \Longrightarrow g_{u_D}(z) = e^{\mu_{gi}(z-1)}$$

The total number of proteins in a cell is $U=U_N+U_D$ and the corresponding probability generating function:

$$g_U(z) = g_{U_N}(z) g_{U_d}(z) = e^{(\lambda+\mu_{gi})(z-1)}$$

The constant μ_{gi} is different for every cell. It is simple and illustrative to consider two special branches of the lineage tree, which we refer to as the "low branch" and the "high branch". In the context of an exponentially dividing population that starts with a single cell and undergoes g rounds of divisions, a branch is an ancestral lineage from any cell in generation g, back to the initial cell. The "low branch" then corresponds to the lineage of the mother cell, which at every division inherited more than half of the protein. The high branch corresponds to the lineage of the "extremal" daughter cell, i.e., the cell that at every division inherited less than half of the protein. These two branches represent the minimal and maximal amounts of achievable pumps in the population, and thus limit the population distribution.

High branch

$\boldsymbol{\mu}_{01} = \lambda$

$\boldsymbol{\mu}_{11} = \lambda + (1-q)\lambda$

$\boldsymbol{\mu}_{21} = \lambda + (1-q)(\lambda + (1-q)\lambda)$

$$\boldsymbol{\mu}_{g1} = \lambda \sum_{i=0}^{n} (1-q)^i = \frac{\lambda}{q}\,(1-(1-q)^{n+1})$$

$$\boldsymbol{\mu}_{\infty 1} = \frac{\lambda}{q}$$

Low branch

$\boldsymbol{\mu}_{01} = \lambda$

$\boldsymbol{\mu}_{12} = \lambda + q\lambda$

$\boldsymbol{\mu}_{24} = \lambda + q(\lambda + q\,\lambda)$

$$\boldsymbol{\mu}_{g2^g} = \lambda \sum_{i=0}^{n} q^i = \frac{\lambda}{1-q}\,(1-q^{n+1})$$

$$\boldsymbol{\mu}_{\infty 2^\infty} = \frac{\lambda}{1-q}$$

The resulting population distribution of protein is a mixture distribution of all the cells in generation *g*. We calculated this analytically using Mathematica for up to 10 generations, and verified by numerical computation (where the protein amount *u* is discretized and the evolution of the discrete approximating distribution $\tilde{P}(u)$ is explicitly evolved forward in time); we also checked the approach to stationarity by doing numerical computations. The timescale for approaching stationarity can be deduced by looking at how mean values μ_{gi} for different cells approach their infinity limit, $g \to \infty$. The time scales to reach steady state and to dilute out are both dependent on q. The number of generations n it takes to reach a value that is a fraction ε of the infinite limit, is:

$$n_q = \frac{\log(\varepsilon)}{\log(q)} - 1$$

We note that this timescale only depends on the partitioning bias q and not on the production rate λ. The same is true for the time it takes to dilute to some fraction f of the maximum value.

$$N_q = \frac{\log(f)}{\log(q)}$$

From these expressions we can calculate the scaling factor that describes how unequal partitioning q changes the timescales compared to even partitioning $q=0.5$. This factor is the same for both the build-up time and the dilution time:

$$\rho_q = \frac{n_q}{n_{0.5}} = \frac{N_q}{N_{0.5}} = \frac{\log(0.5)}{\log(q)}$$

Extracting model parameters from data

The proposed model is the simplest model that captures the effects of biased partitioning in an exponentially growing population. The model makes a number of assumptions and idealizations, which are likely not fulfilled, for example: *(i),* the efflux pump production process is likely not strictly Poisson; *(ii)*, the production of pumps is likely actively regulated, including both feedback and regulation due to external inputs; *(iii),* partitioning of individual pumps may not be independent. Nevertheless, as the model provides a controlled baseline to explore the effects of biased vs unbiased partitioning, we apply it to the AcrB-GFP fusion data. For AcrB-GFP, the measured partitioning asymmetry is the strongest, and AcrB-GFP is the substrate-binding subunit of AcrAB-TolC, and thus a specific marker for AcrAB-TolC. We note that in linking the model (which describes protein counts) and the data (which measures total fluorescence intensity), there is an unknown proportionality constant. While this constant does not

affect the mean of the distribution except for redefining the units of measurement, it affects the magnitude of the Poisson noise components. The estimation of the partitioning bias q and the production rate λ, as described below, is unaffected by this. The quantitative prediction for the distribution of pump amounts in the population depends on the magnitude of the Poisson noise, but the effect is likely small if the population heterogeneity due to partitioning bias is larger than due to the stochastic production. The fact that we can reliably observe strong and consistent differences between mother and daughter cells in the experiment, despite stochastic gene expression in individual cells, strongly suggests that the bias is the dominant source of heterogeneity.

Four quantities can be extracted from data that together provide the means to infer the model parameters and validate the model. Two parameters that are explicitly present in the model are the protein production rate λ and the partitioning bias q. We call these parameters *local*, because they can be measured at each individual division event for every cell. In contrast, there are two *global* quantities: the final (steady-state) level of cell fluorescence, n; and the time scale factor, ρ, by which q affects the dynamics of the system. These quantities can be measured from fluorescence traces of mother (M) cells, i.e., we can extract ρ and ν for each lineage. These values are also directly computable from the model and can thus be compared to data. In principle it is possible to estimate model parameters (q,λ) from either local or global quantities. While estimation-wise it is more stable to infer (q,λ) from a mix of local and global measurements, we decided to make direct estimates of (q,λ) based on local measurements alone, e.g., using only local information on individual cell divisions, and then to use the model to predict the global parameters and compare the predictions to data as means of model validation. The estimation procedure described below can be used identically on both, the efflux pump fusion fluorescence channel or the constitutively expressed cytoplasmic fluorescence protein (control).

Estimating production rate λ

We estimate the production rate λ by fitting a straight line to the total fluorescence at all the time points within a single cell cycle. An estimate for λ is obtained by computing the per-cell-cycle increase in fluorescence using this linear model and the production time equal to the estimated number of imaging frames between the two division events. This measure is an approximation for three reasons: first, because of the underlying assumption that the increase in fluorescence is linear; second, because the frame-rate-induced granularity limits the precision by which we can determine the cell cycle duration; and third, because of the intrinsic experimental noise in fluorescence measurements.

Estimating partitioning bias q

Assuming that Poisson fluctuations are moderate and that λ has been extracted for each division event in the mother cell lineage as described above, we use expressions for the means μ_g and μ_{g+1} to estimate q. Let f_g be the fluorescence proportional to the average number of pumps in generation g in the mother, $f_g \propto \mu_{g2^g}$. For most analyses, a background correction that accounts for the relative inhomogeneities in space and time of the light source is sufficient. However when combining λ and f measurements to infer our model parameters it becomes important to have an accurate estimate of the background

fluorescence of a cell without fluorescent marker (within-cell background); this is because such background is, by construction, removed from λ, and since λ and *f* both enter the expressions for partitioning, we thus need to remove such background also from *f*. To this end we assume a model for the within-cell background (B_{in}) that is a linear function of the measured background outside of the cell (B_{out}) for each image: $B_{in,g}=a_1 B_{out,g}+ a_2$. The constants a_1, a_2 are assumed equal for all cells and all times. Then the following relation should hold for the mother cell after division: $f_{g+1} - B_{in,g+1} = q(f_g - B_{in,g}) + \lambda_g$, for the daughter we have: $f_{g+1} - B_{in,g+1} = (1-q)(f_g - B_{in,g}) + \lambda_g$. Using measured data form both mother and daughter cells of each division event (f_g, λ_g, background measurements outside of the cell) we fit the parameters (q, a_1, a_2) using nonlinear regression (MATLAB nlinfit) with least squares, by predicting the fluorescence at time ($g+1$). This gives an estimate of q ($q^* = 0.62$ reported in the main text) when extracted jointly from all recorded division events, which is consistent with extracting q separately for each lineage and reporting the average. The error bar on the value of q reports the std over fits to individual lineages.

Prediction of the steady state level in mother cells

The final steady-state level n is estimated for each lineage by averaging over the total fluorescence just after cell division in the last 5 observed generations. This is compared to the model prediction, $\rightarrow \frac{\lambda}{1-q}$, using per-lineage estimates for λ and q. Given that the model is making global predictions based on the locally inferred quantities, the match is surprisingly good, as is the match between predictions and data, averaged across lineages, reported in Figure 4D. It is also possible to use the measured steady state levels n in combination with locally inferred q to compute the production λ, and compare that with the directly measured production rates, which also exhibits an excellent match (data not shown).

Estimating decay time $t_{1/2}$

We measured the time it takes for the fluorescence to decay by half in a strain expressing AcrB-GFP, and as a control in a strain expressing cytosolic GFP, using the data from the pulse-chase experiment of Figure 1. To estimate these values we fit an exponential to the 140min interval in the pulse-chase experiment, chosen as follows. The first time point is selected to be 60min after the end of induction, where we can observe the start of the decay. The last point was selected to be 200min after the end of induction; until this time point the asymmetry in AcrB-GFP remains constant, and the new pole of the mother cell remains above the background level of fluorescence, such that quantities of interest can be estimated reliably. In this same time interval, 93% of the cytosolic GFP in the control strain has diluted out. Beyond 200min post induction, the new mother cell pole in the AcrB-GFP channel is indistinguishable from the background, and the asymmetry between cell halves seems to be reduced; this process appears distinctly slower and is not captured within our model. The error bar of the value of $t_{1/2}$ is estimated by bootstrapping, as std over independent fits of $t_{1/2}$ over random halves of the data.

Predicting the factor ρ, affecting decay and accumulation

The model predicts a time factor $\rho = \log(0.5) / \log(q)$ that captures how the dynamics of a system is affected by unequal partitioning compared to even partitioning. This factor is larger than one in all cases where the mother cell retains more protein ($q > 0.5$). For our estimate of $q^* = 0.62$, $\rho = \log(0.5) / \log(0.62) = 1.45$. In the main text we report this factor as the ratio between the fluorescence decay time and the generation time and find that for the AcrB-GFP $t_{1/2} / t_g = 1.39 \pm 0.19$, while for cytosolic GFP, where the expectation is 1, we find $t_{1/2} / t_g = 1.06 \pm 0.09$. We can also calculate ρ from the accumulation phase of the pulse-chase experiment. In this case the induction dynamics are unknown, but we can make a crude estimate by looking at what time point the half-maximal fluorescence is reached and calculate ρ from the ratio between the unequally partitioned AcrB-GFP and the evenly partitioned cytosolic GFP; we find $t_{1/2} / t_g = 1.45 \pm 0.04$, which again agrees with the model prediction.

Fig. S1.

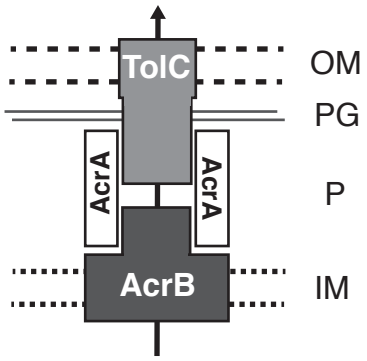

Fig. S1. Schematic of AcrAB-TolC.

Schematic of AcrAB-TolC. OM - outer membrane, PG – peptidoglycan, P - periplasm, IM - inner membrane. In *E. coli*, the only outer membrane factor interacting with several efflux and export systems with highly diverse functions is TolC (*12*). The relationship between TolC and its interaction partners, which are comprised of several ABC, MFS and RND-type efflux substrate binding and periplasmatic fusion proteins, as well as several small peptide export systems, is non-stoichiometric. TolC is regulated independently and is located on the *E. coli* chromosome in an operon with three genes of unknown function, while many of the efflux systems are often organized as tandem operons. Thus, the role of stoichiometry of different interaction partners for ternary complex formation remains to be elucidated, while TolC appears to be the limiting factor for formation of the many different types of ternary complexes. Recently, transporter exchange was suggested as one mechanism in which competing RND-type pumps can form ternary complexes with TolC (*35*), and the formation of AcrAB-TolC could thus depend nontrivially on other TolC-containing complexes. While AcrAB appears to be the only RND-type transporter that is constitutively expressed under laboratory conditions (*13*), the presence of AcrAB-TolC complexes could be influenced by complex steady states among different possible tripartite complexes (*35*).

Fig. S2.

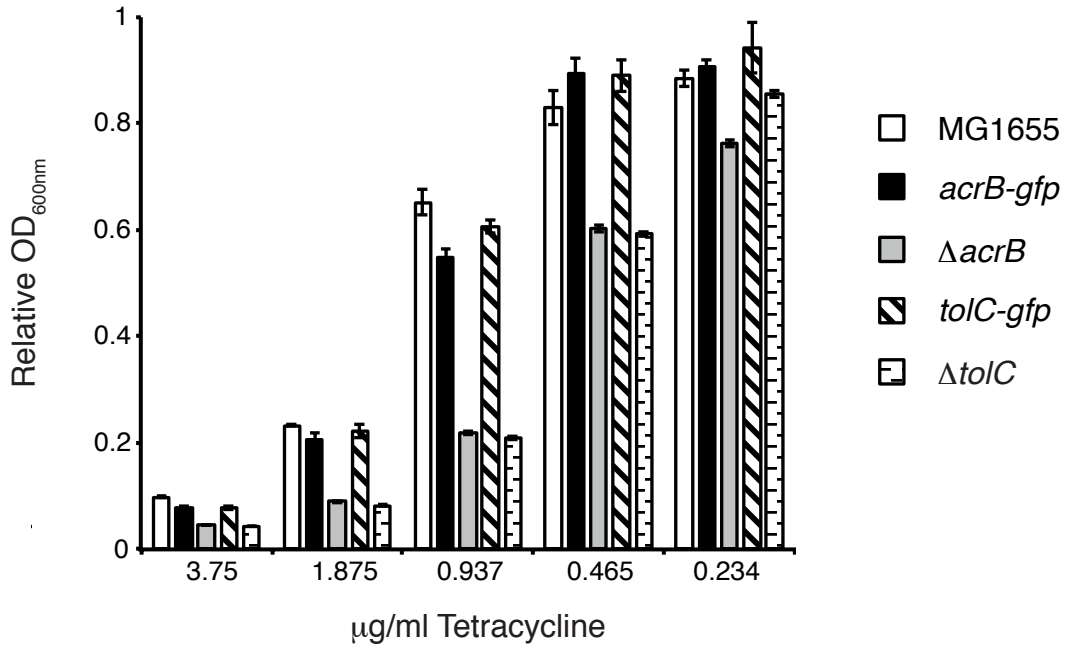

Fig. S2. Functionality of strains expressing efflux pump protein fusions assayed by MIC.

The susceptibility of strains towards tetracycline was determined by serial dilution, and strains were measured in triplicates. Plotted is optical density after 20h relative to an untreated control. The drug sensitivity of strains expressing chromosomally encoded and natively expressed AcrB-GFP or TolC-GFP is largely indistinguishable from the reference strain MG1655. Deletion of either the substrate-binding subunit *acrB* or the outer-membrane component *tolC* yields strains of similarly increased drug sensitivity. Error bars=+/-1 SE.

Fig. S3.

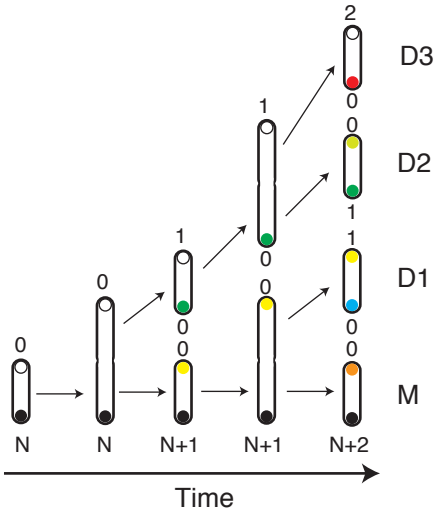

Fig. S3. Pole age segregation in *Escherichia coli*

The poles of an *E. coli* cell can be used to identify an individual. Each individual cell has an old cell pole arising from a past cell division event of age N. The other cell pole is naive, i.e. it formed during the last cell division event, age zero. After each cell division preexisting poles increase in age by one. We term the two sister cells emerging from the cell division of a cell with pole age N as mother and daughter. Mothers inherit the increasingly old pole (full circle) and daughters the new cell pole (empty circle). Colors are used to tag and track individual poles over generations.

Fig. S4.

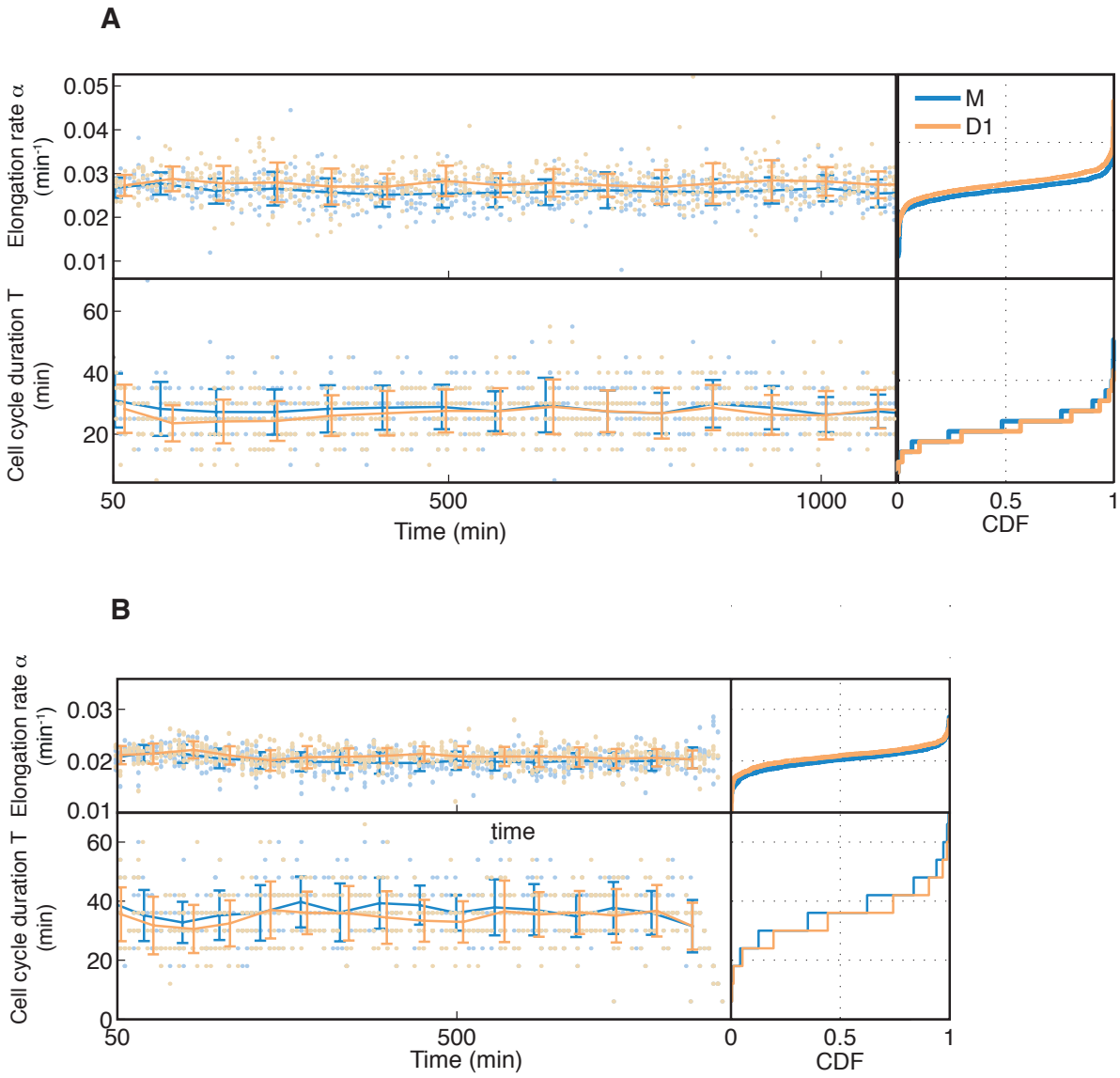

Fig. S4. Robust growth of strains during cultivation in mother machine.

Elongation rate (α) and cell cycle duration (T) measured for individual mother and daughter cells growing inside a mother machine. *E. coli* grows robustly under these conditions, and no cumulative effects of prolonged cultivation inside the microfluidic device are observed. (A) Strain expressing AcrB-GFP and cytoplasmic mCherry. (B) Reference strain expressing cytoplasmic mCherry. Lines - averages, error bars - STD. On the right, cumulative distribution functions (CDF) for α and T.

Fig. S5.

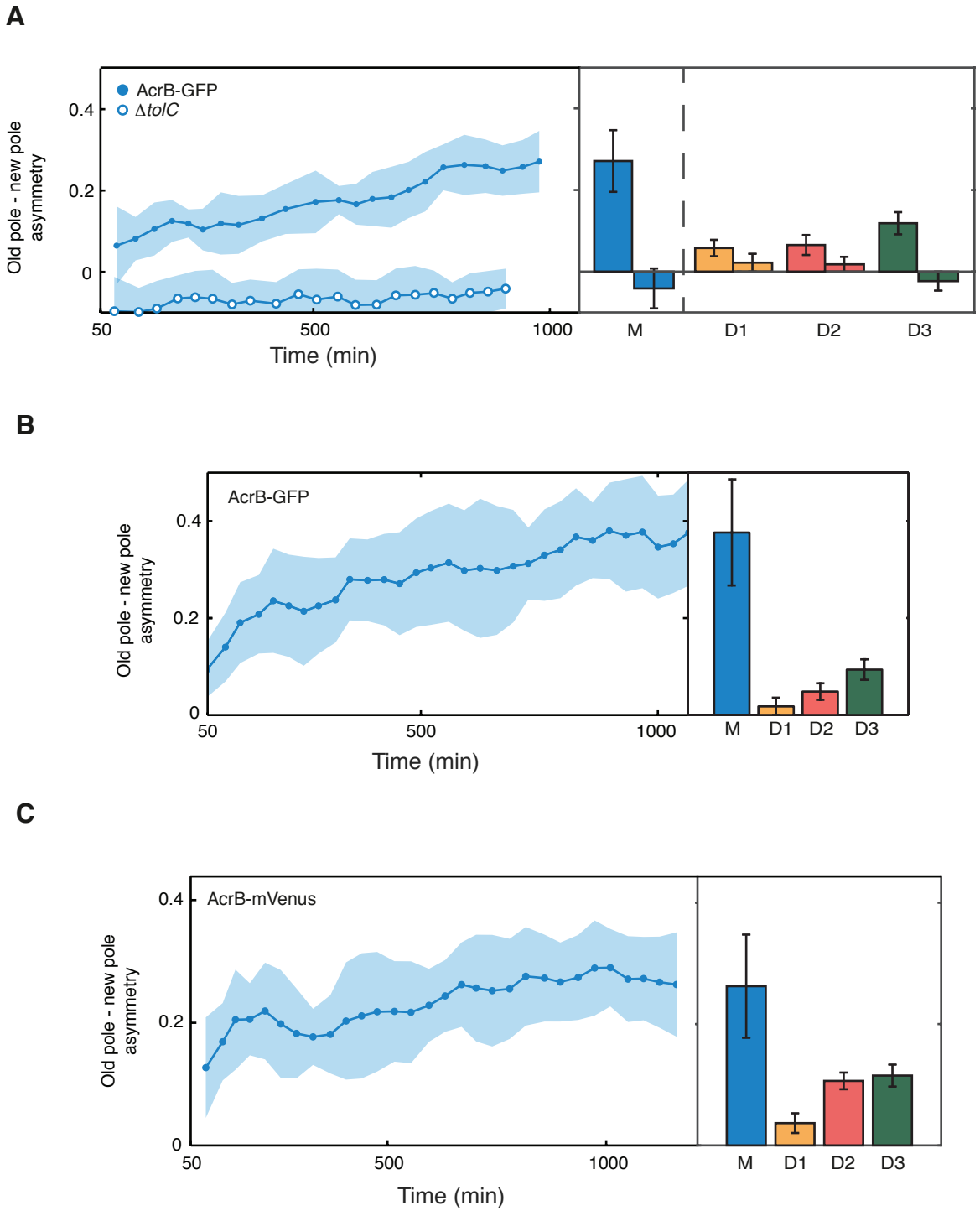
A
AcrB-GFP
ΔtolC
Old pole - new pole asymmetry
0.4
0.2
0
50
500
1000
Time (min)
M
D1
D2
D3
B
AcrB-GFP
Old pole - new pole asymmetry
0.4
0.2
0
50
500
1000
Time (min)
M
D1
D2
D3
C
AcrB-mVenus
Old pole - new pole asymmetry
0.4
0.2
0
50
500
1000
Time (min)
M
D1
D2
D3

Fig. S5. Polar localization and accumulation of AcrB-GFP at old cell poles

A selection of replicate experiments for the Figure 1D (A) Replicate with both AcrB-GFP fusion and Δ*tolC* strains. 23 and 17 colonies respectively (B) Replicate with AcrB-GFP strain 22 colonies. (C) Replicate with AcrB-mVenus strain, 16 colonies. Left panels: within-cell fluorescence asymmetry in M cells expressing AcrB-GFP, quantified as (old cell half – new cell half)/(whole cell). Smoothed over three time-bins; dots = mean generation times, envelope = STD over cells. Right panels: bar for M shows final asymmetry, bars for D1/D2/D3 are time averages throughout entire experiment. Error bars = ±1 STD).

Fig. S6.

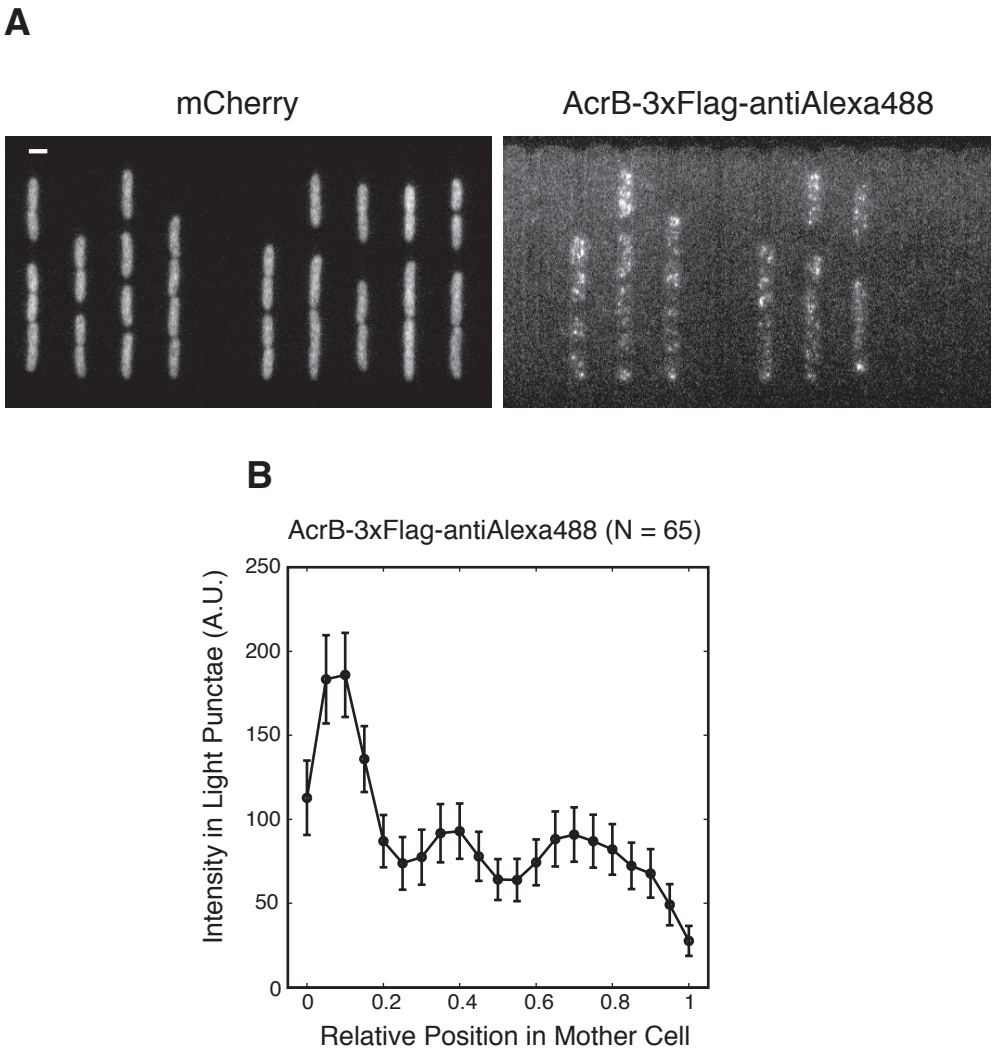

Fig. S6. Polar localization of AcrB-3xFlag in mother cells

(A) Strains expressing chromosomally and natively expressed AcrB-3xFlag and cytoplasmic mCherry were co-cultured with a reference strain expressing cytoplasmic mCherry only for 14h, and treated for immunostaining using a primary anti-Flag-Alexa488 antibody. If antibody labeling of 3xFlag epitopes is specific, all-or-nothing staining patterns of cells inside channels is to be expected. Shown is an unprocessed maximum intensity projection of Z-stacks containing 7 stacks of channels with all-or-nothing staining. AcrB-3xFlag-anti-Alexa488 appears as punctate patterns along the cell periphery. Unlike freely diffusion molecules, antibodies strongly bind to 3xFlag epitopes, and thus cells closer to the open end of channels are more stained than cells at the bottom due to oversaturation. Scale bar = 2μm.

(B) Quantification of AcrB-3xFlag-anti-Alexa488 localization in mother cells (N=65 cells). The x-axis shows the relative distance of fluorescent foci from the old pole scaled to 1 (0 = old pole, 1=new pole). Error bars=+/-1 SE.

Fig. S7.

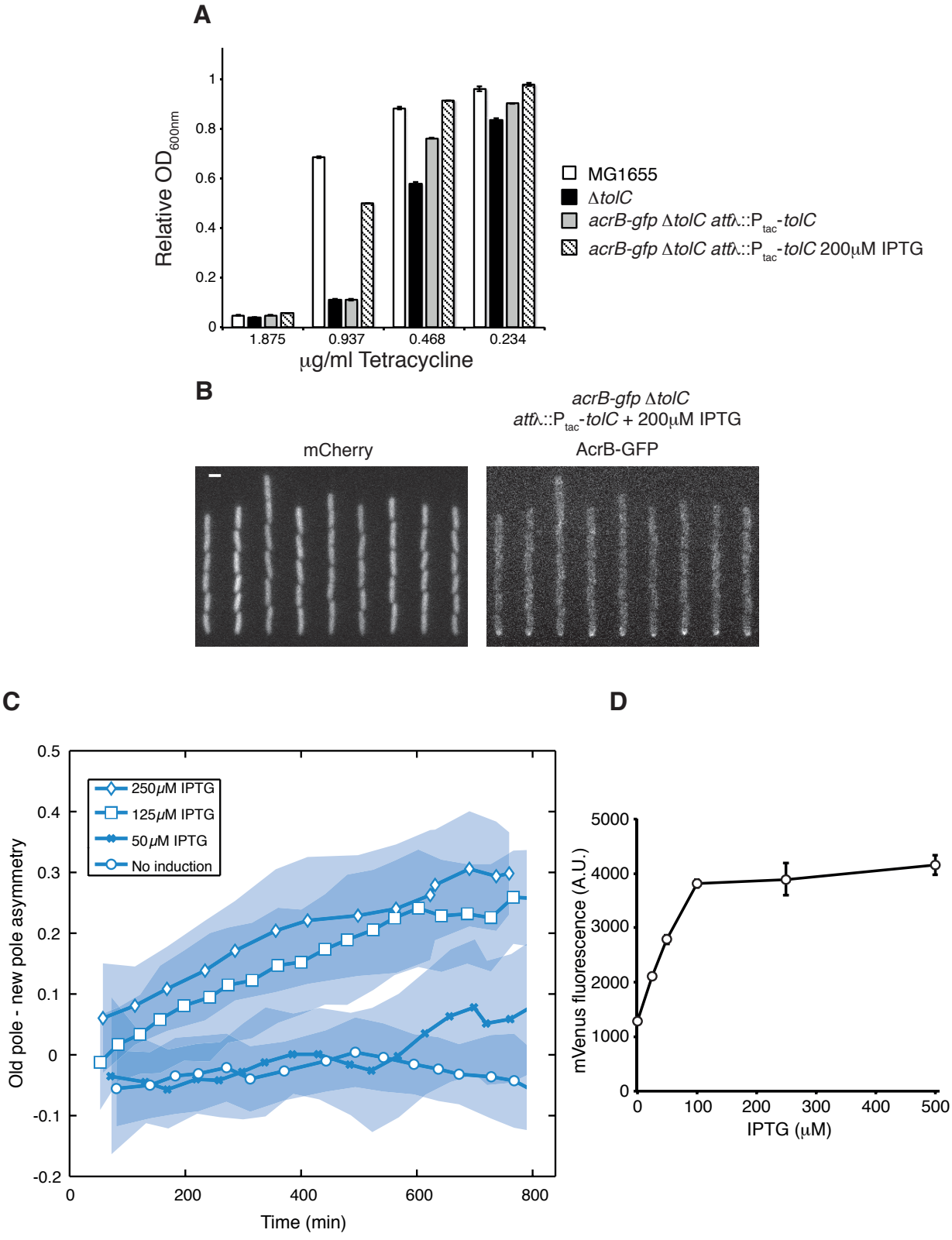
A
Relative OD600nm
1
0.8
0.6
0.4
0.2
0
1.875
0.937
0.468
0.234
μg/ml Tetracycline
MG1655
ΔtolC
acrB-gfp ΔtolC attλ::Ptac-tolC
acrB-gfp ΔtolC attλ::Ptac-tolC 200μM IPTG
B
acrB-gfp ΔtolC
attλ::Ptac-tolC + 200μM IPTG
mCherry
AcrB-GFP
C
Old pole - new pole asymmetry
0.5
0.4
0.3
0.2
0.1
0
-0.1
-0.2
0
200
400
600
800
Time (min)
250μM IPTG
125μM IPTG
50μM IPTG
No induction
D
mVenus fluorescence (A.U.)
5000
4000
3000
2000
1000
0
0
100
200
300
400
500
IPTG (μM)

Fig. S7. Complementation of *tolC* in trans

TolC was expressed from a single-copy IPTG-inducible chromosomal gene (*att*λ::P_{tac}-*tolC*; see Material and Methods) in an *acrB-gfp* Δ*tolC* strain, and expressed by adding 200μM IPTG.

(A) TolC complementation with 200μM IPTG restores wild type-levels of tetracycline sensitivity of *acrB-gfp* Δ*tolC* strain, determined by serial dilution. Strains were measured in triplicates. Plotted is optical density after 20h relative to an untreated control. Error bars=+/-1 SE.

(B) Polar localization of AcrB-GFP after 900min of growth inside a mother machine in the presence of 200μM IPTG. Left, mCherry; right, AcrB-GFP. Scale bar = 2μm.

C) Induction of TolC from *att*λ::P_{tac}-*tolC* with different concentrations of IPTG added at time zero to the microfluidics growth medium, and the resulting AcrAB-GFP within-cell asymmetry in mother cells. Markers indicate mean over colonies per generation, envelope one STD over cells. Number of colonies per induction level: No IPTG, 21; 50μM IPTG, 20; 125μM IPTG, 24; 250 μM IPTG, 22.

(D) Induction curve of *att*λ::P_{tac}-*mVenus*. Plotted fluorescence values are derived from each five replicate cultures growing at 0, 25, 50, 100, 250 and 500μM IPTG after 4.5h of growth. P_{tac} induction is saturated at 100μM IPTG.

Fig. S8.

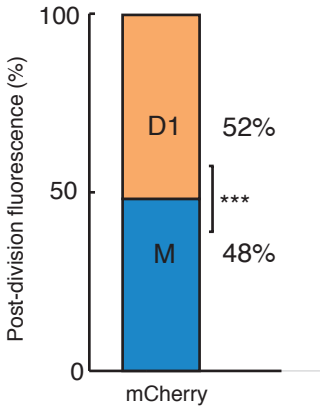

Fig. S8. Partitioning of cytosolic mCherry.

Soluble cytoplasmatic mCherry expressed from the chromosome is approximately evenly distributed at cell division. The small partitioning bias is significant ($p < 10^{-4}$, t-test), but of opposite sign than the much larger bias in AcrB-GFP reported in the main text. The reported small bias is likely attributable to a small growth rate difference between M and D1 cells.

Fig. S9.

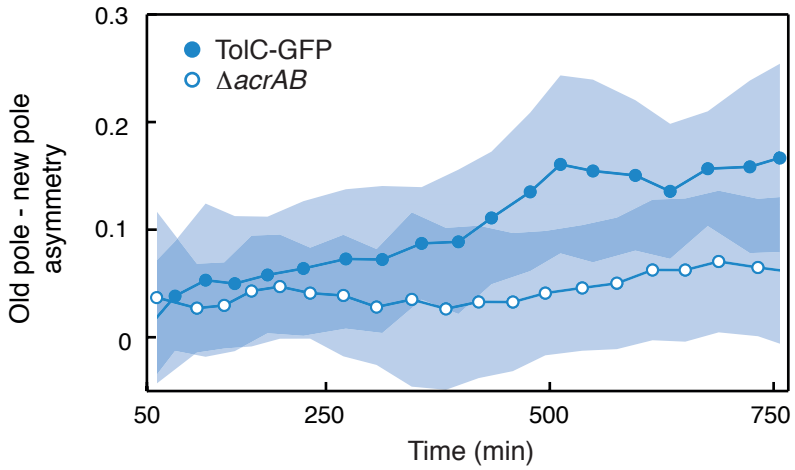

Fig. S9. TolC-GFP accumulates at old cell poles.

Within-cell asymmetry in mother cells expressing TolC-GFP in the presence or absence of AcrAB, quantified as (old cell half – new cell half)/(whole cell) fluorescence and smoothed over three time-bins; dots = mean generation times, shade = STD over cells. Plotting conventions are the same as in Figure 1 of the main text.

Fig. S10.

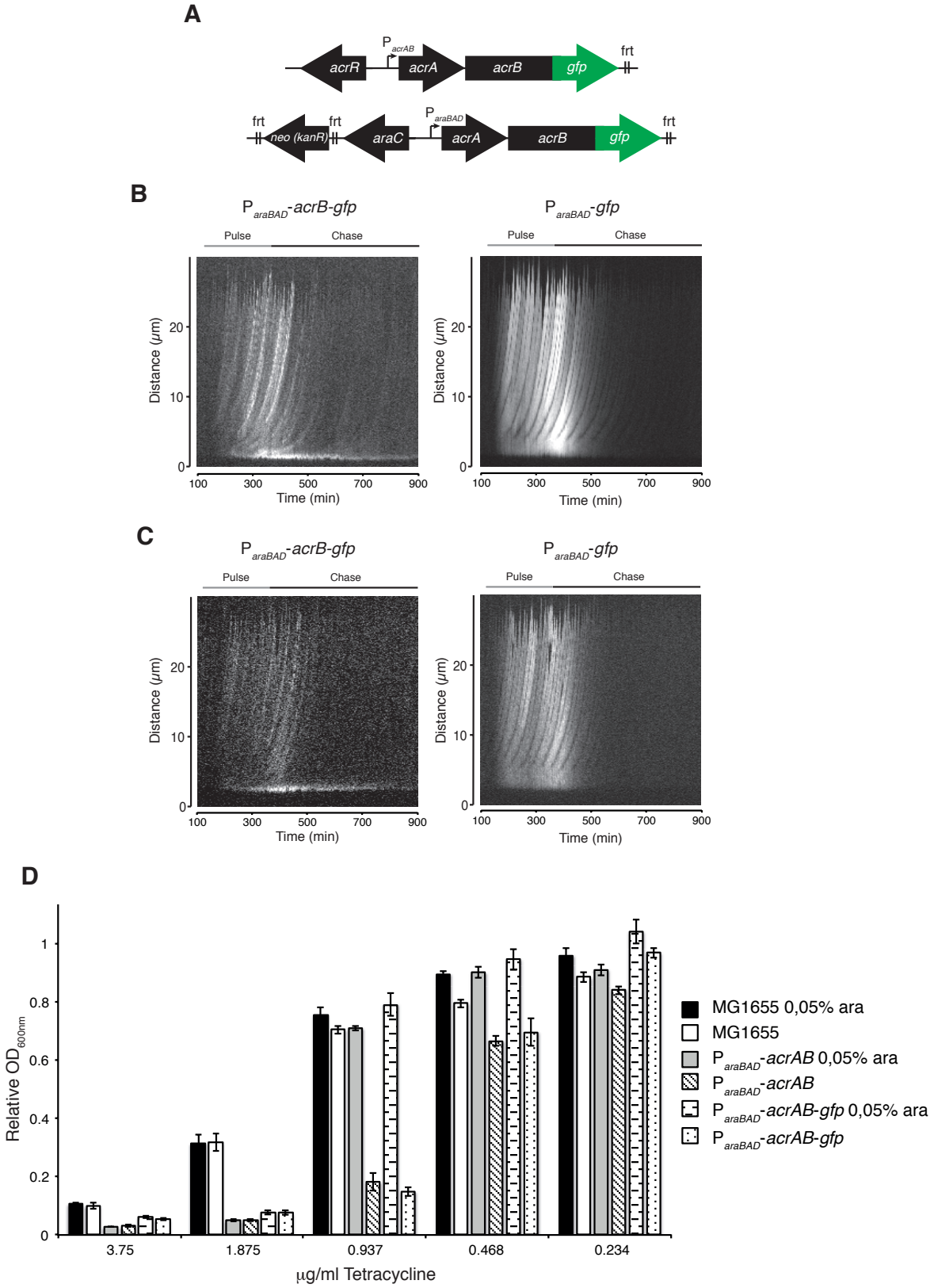
A
P acrAB
acrR
acrA
acrB
gfp
frt
frt
frt
neo (kanR)
araC
P araBAD
acrA
acrB
gfp
frt
B
P araBAD-acrB-gfp
P araBAD-gfp
Pulse
Chase
Distance (μm)
Time (min)
C
P araBAD-acrB-gfp
P araBAD-gfp
Pulse
Chase
Distance (μm)
Time (min)
D
Relative OD 600nm
μg/ml Tetracycline
3.75
1.875
0.937
0.468
0.234
MG1655 0,05% ara
MG1655
P araBAD-acrAB 0,05% ara
P araBAD-acrAB
P araBAD-acrAB-gfp 0,05% ara
P araBAD-acrAB-gfp

Fig. S10. Pulse-chase of P_{araBAD}-*acrB-gfp* and P_{araBAD}-*gfp*.

(A) Schematic of the genetic construct: *acrAB-gfp* locus in native configuration and modified with an arabinose-inducible P_{araBAD} cassette. A cassette consisting of an outward-facing kanamycin marker flanked with FLP-recombinase targeting sites (frt), the full *araC* open reading frame, and the native P_{araBAD} promoter was inserted upstream of *acrAB-gfp*. The insertion removes *acrR* and the entire *acrAB* promoter, and fuses P_{araBAD} transcriptionally to *acrAB*.

(B) and (C) Kymographs of pulse-chase in mother machine. Shown are kymographs of representative growth channels of a pulse-chase experiment: P_{araBAD}-*acrB-gfp* (left) and P_{araBAD}-*gfp* (right). To transiently express AcrB-GFP, 0.05% L-arabinose was added to the microfluidic growth medium at 120min, and washed out at 360min. B and C show data from independent replicate experiments.

(D) Arabinose-dependent tetracycline sensitivity. Strains used for pulse-chase experiments were tested for the functionality of AcrAB-TolC by measuring arabinose-dependent sensitivity to tetracycline. Addition of 0.05% arabinose led to nearly wild type levels of tetracycline sensitivity of P_{araBAD}-*acrB-gfp* or P_{araBAD}-*acrB* strains. Error bars=+/-1 SE.

Fig. 11.

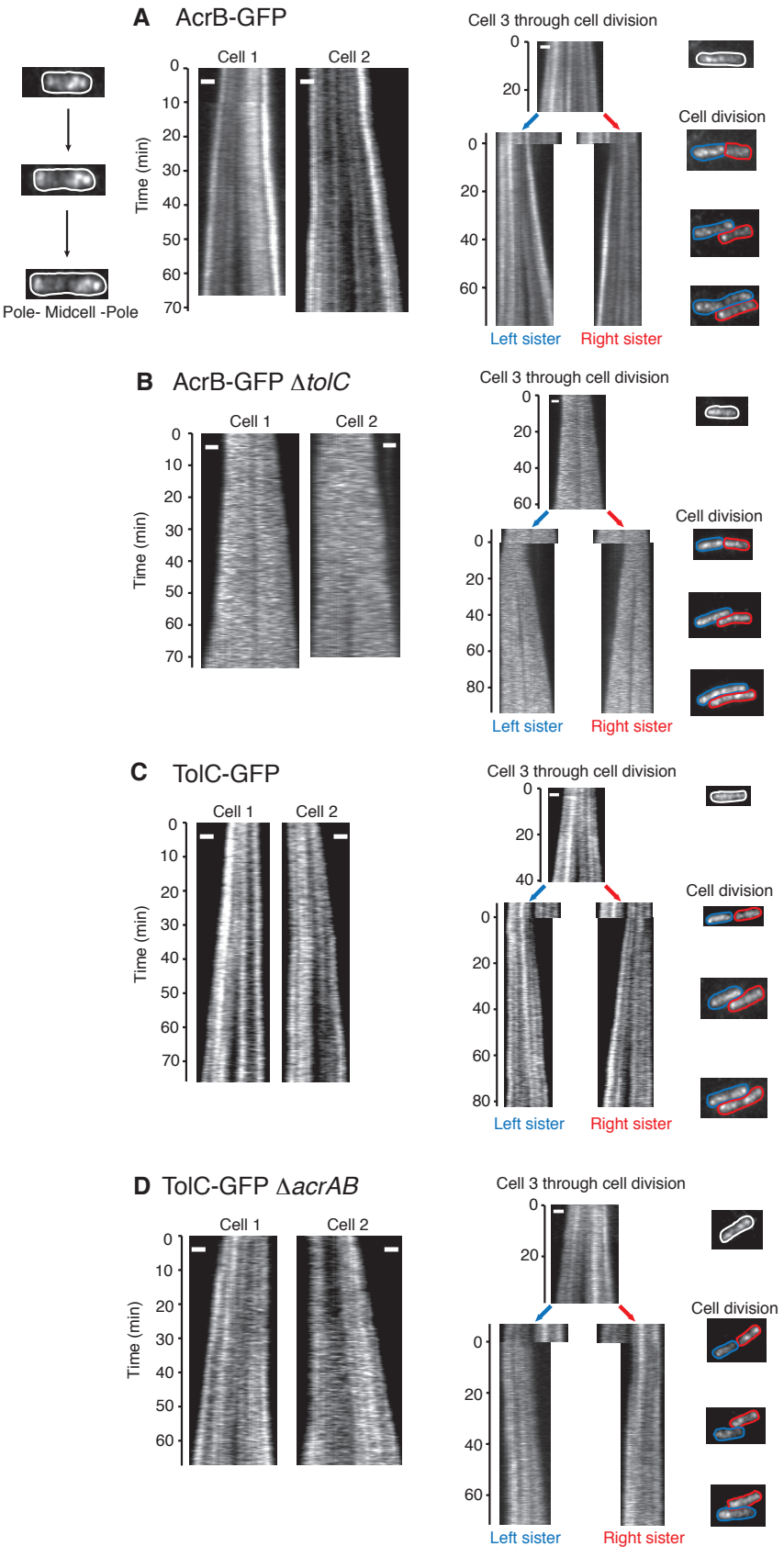
A AcrB-GFP
Pole- Midcell -Pole
Cell 1
Cell 2
Time (min)
Cell 3 through cell division
Cell division
Left sister
Right sister
B AcrB-GFP ΔtolC
C TolC-GFP
D TolC-GFP ΔacrAB

Fig. S11. AcrB-GFP and TolC-GFP imaged with TIRFm.

Cells expressing (A) AcrB-GFP in a reference strain background, (B) AcrB-GFP in a Δ*tolC* deletion strain, (C) TolC-GFP in a reference strain and (D) TolC-GFP in a Δ*acrAB* deletion strain. Kymograph representations show the persistence of a feature over space and time, and vertical lines correspond to stationary objects, while oblique lines correspond to moving objects. In the presence of TolC, AcrB-GFP forms long vertical lines representing stationary clusters that move away from each other by cell elongation growth, which is absent in polar regions (*36*). Thus, older clusters are at the edge of the active zone of growth and segregate in pole-proximal regions, and appear brighter or larger, potentially due to cluster growth over time. Based on our observations, fully assembled ternary complexes are trapped in the cell envelope and slowly separate by incorporation of new material (A). In the absence of TolC, no stationary AcrB-GFP clusters are visible, which suggests that AcrB-GFP is freely moving in the inner membrane ((B), as suggested by (*35*)). Trapping of AcrAB-TolC is most likely mediated by TolC protruding through the peptidoglycan layer, which is a rigid polymer that could render AcrAB-TolC stationary. TolC-GFP formed similar clusters, which appeared less defined in the absence of AcrAB (D).

Kymographs of cells 1 and 2 of each strain approximate one cell cycle, kymographs for cell 3 are assembled over two consecutive cell cycles, with colors indicating the two sister cells. White scale bars = 1μm. Cell outlines mark cell bodies. Time axis for all cells 3 is reset to 0 at cell division.

Fig. S12.

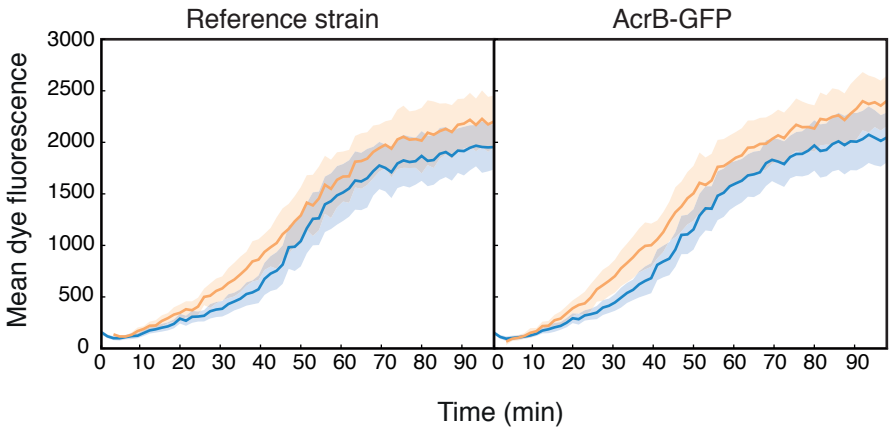

Fig. S12. Efflux activity comparisons.

H33342 dye uptake profiles of strains expressing AcrB-GFP, and a reference strain without fluorescent efflux protein fusion measured side-by-side in the same microfluidic experiment indicate that AcrB-GFP does not affect H33342 efflux in single cells. Envelopes = STD over cells.

Fig. S13.

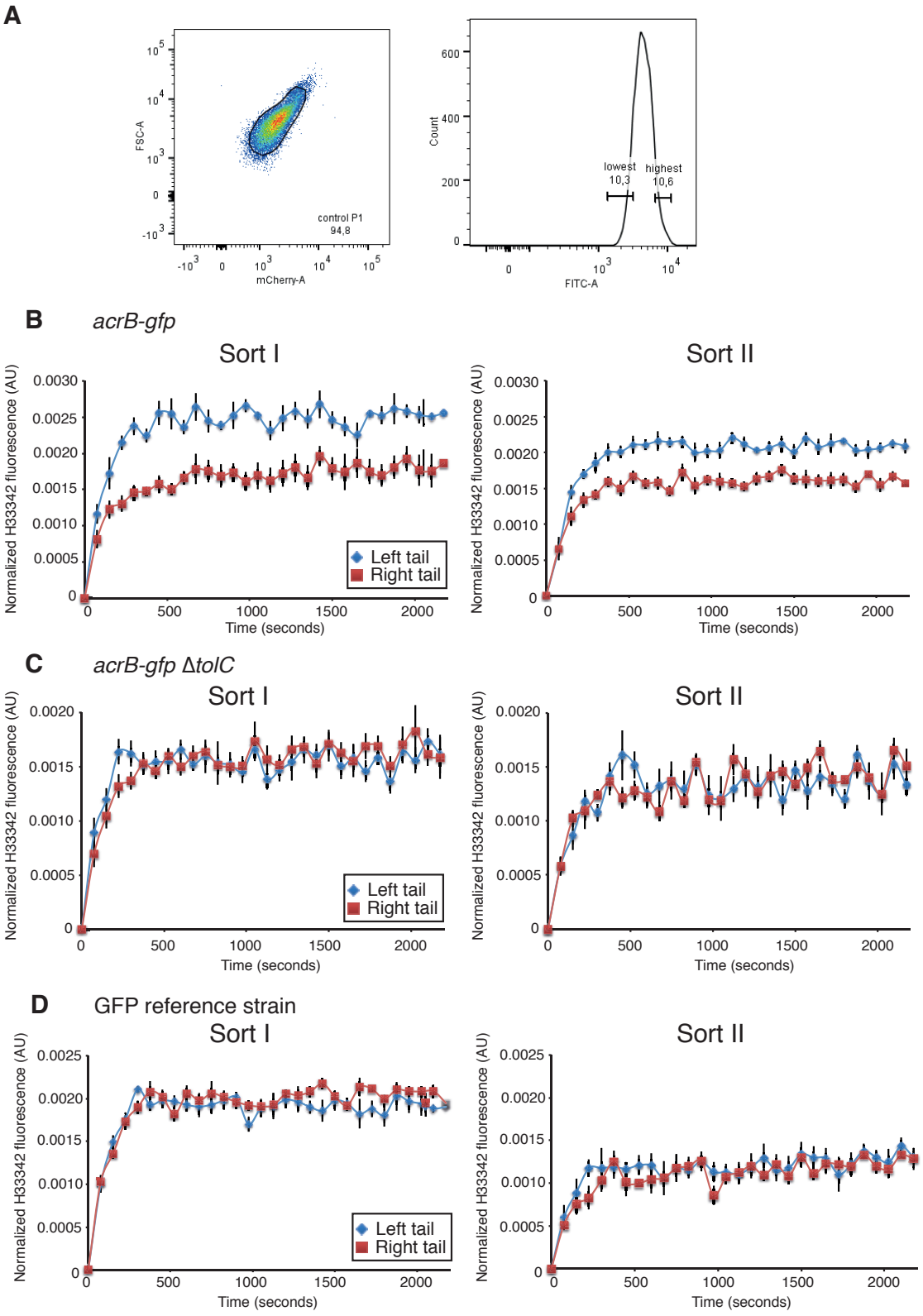
A
FSC-A
mCherry-A
control P1
94,8
Count
FITC-A
lowest
10,3
highest
10,6
B
acrB-gfp
Sort I
Sort II
Normalized H33342 fluorescence (AU)
Time (seconds)
Left tail
Right tail
C
acrB-gfp ΔtolC
Sort I
Sort II
Normalized H33342 fluorescence (AU)
Time (seconds)
Left tail
Right tail
D
GFP reference strain
Sort I
Sort II
Normalized H33342 fluorescence (AU)
Time (seconds)
Left tail
Right tail

Fig. S13. AcrB-GFP fluorescence is a proxy for efflux activity at the population level.

Shown are two independent sorting experiments using FACS, with independent cultures being sorted on two different days. Cells were sorted according to AcrB-GFP signal, and assayed for efflux activity in a 96-well microtiter plate assay.
(A) Representative forward scatter (FSC) and mCherry scatter plot of an *E. coli* population, and representative distribution of AcrB-GFP signal after the population was gated on FSC and mCherry. Depicted sorting gates are not up to scale.
(B through D) Efflux activity of sorted cells: (B) *acrB-gfp* left and right tails, C) *acrB-gfp* Δ*tolC* left and right tails, and (D) of reference strain sorted on left and right tails of constitutively expressed GFP. Error bars=+/-1 SE. Mean fluorescence values (a.u.) of triplicate experiments measured with a FACS analyzer for an *acrB-gfp* strain is 81.5±0.3, and 141.7±2.0 for an *acrB-gfp* Δ*tolC* strain.

Fig. S14.

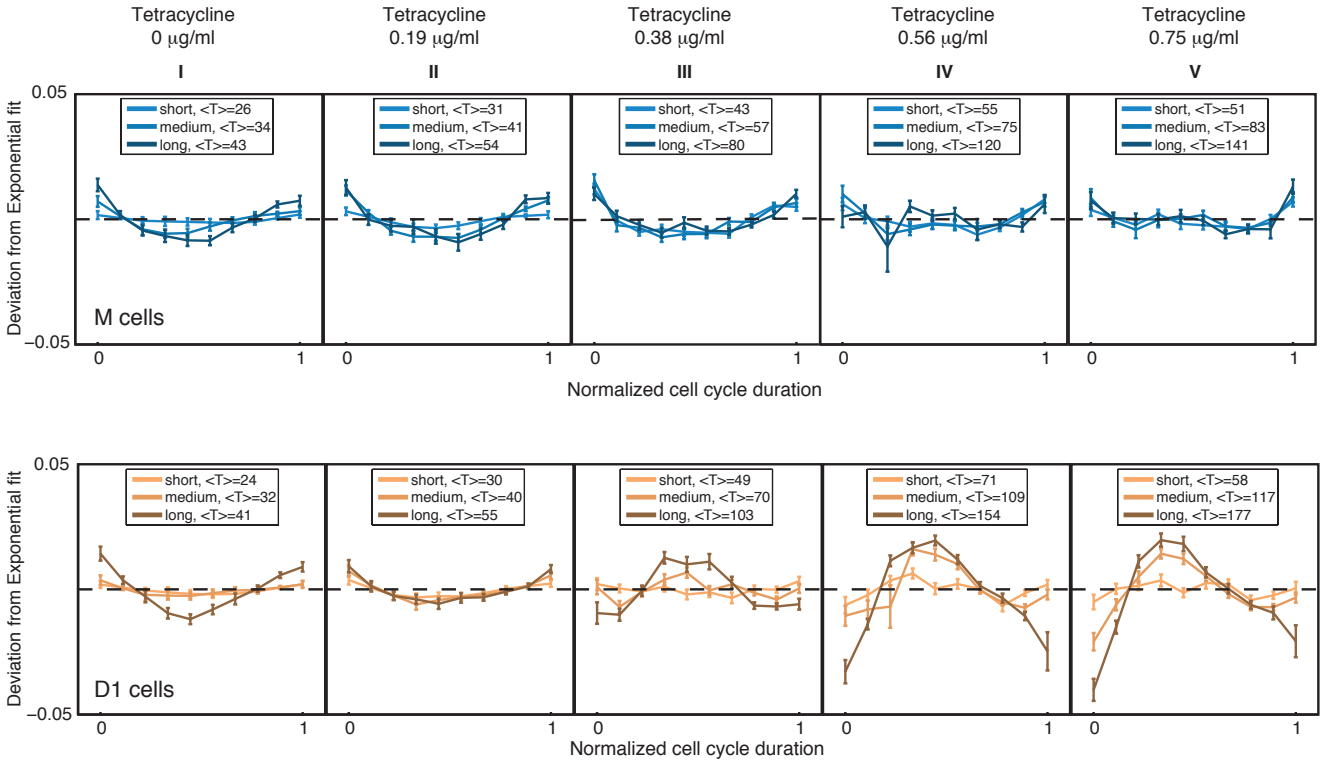

Fig. S14. Deviation from exponential elongation in the presence of tetracycline.

Cell cycle duration between two successive cell division events was normalized between 0 (beginning of the cycle, just after division) and 1 (end of the cycle, just prior to division). Cell length measurements were compared to the expectation of exponential growth at 10 points in this interval. This was done by first fitting a line through the logarithm of the cell length in each cell cycle for every individual cell, and then by computing the differences between the exponential fit and the actual data. These differences are grouped according to cell cycle duration T, into the shortest, middle and longest 33% of cells. Within each group across cells the mean and standard error of the difference between data and the exponential elongation model are calculated and shown in the figure. For true exponential growth, small deviations due to measurement noise average out over many cells, resulting in a nearly straight horizontal line. If single-cell elongation is not well described by a single exponential, there are systematic deviations that do not average out. For example, the concave deviation at high antibiotic concentrations for daughter cells shows that growth tends to slow down just after and just prior to cell division relative to the exponential elongation expectation, and speeds up in the middle of the cycle. Mother cell (M) data is plotted in blue, daughter cell (D1) data in orange. Data is pooled over 3 experiments and measured strains (AcrB-GFP and reference strain expressing cytoplasmic mCherry only). Number of cells per interval for M: I-390; II-630; III-435; IV-326; V-237; and for D1: I-391; II-634; III-438; IV-315; V-232. Error bars=+/-1 SE.

Fig. S15.

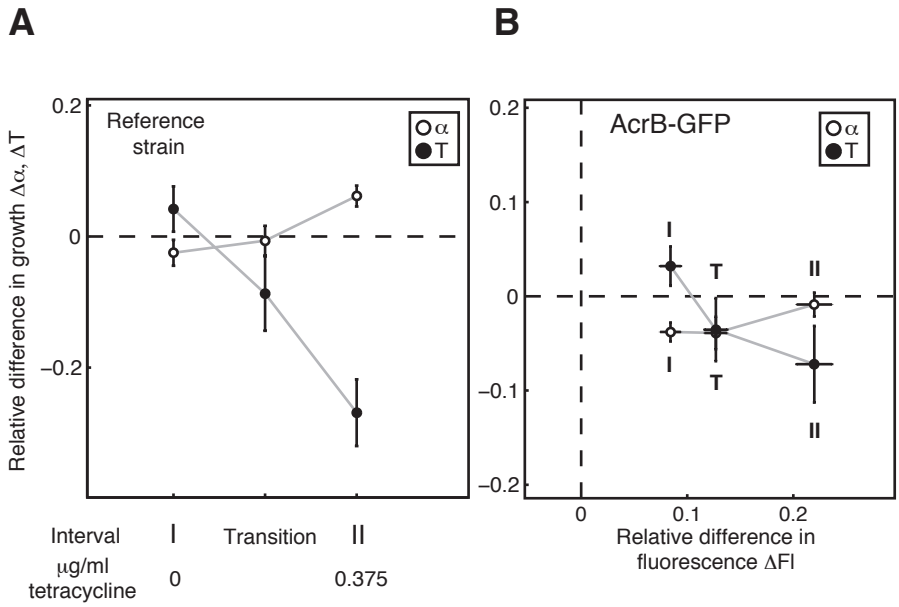

Fig. S15. Exposure to a single concentration of tetracycline.

Difference in growth between M and D1 cells in (A) reference strain expressing cytoplasmic mCherry and (B) AcrB-GFP exposed to a single dosage of tetracycline (0.375μg/ml). Interval I: no antibiotic for 360min; Transition (T): first 300min with 0.375μg/ml tetracycline; II: last 300min with 0.375 μg/ml tetracycline. Average and standard error of difference in growth ((M-D1)/M) between sister M and D1 cells is plotted in green for a and in purple for T. Qualitatively, the trends of M-D1 growth differences are similar to the multi-exposure experiments described in the main text. Quantitative differences to the multi-exposure experiment might be explained by priming effects of stepwise exposures to low antibiotic concentrations. Error bars=+/-1 SE.

Fig. S16.

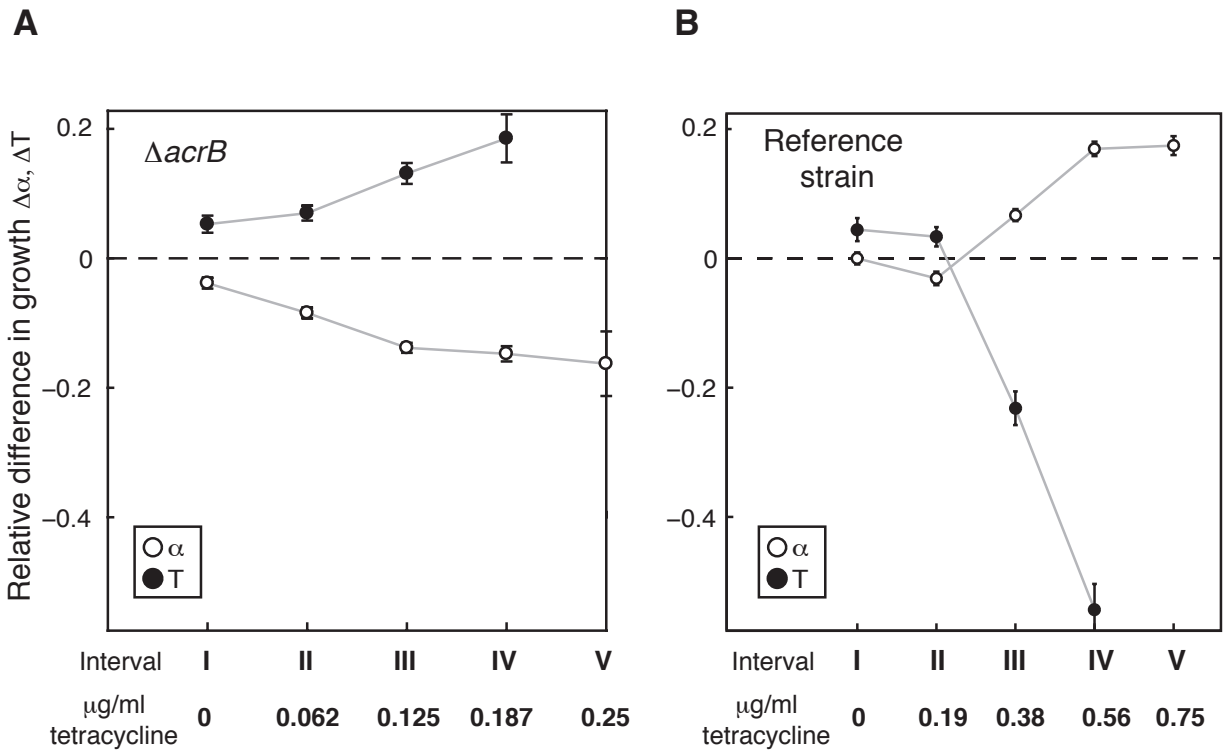

Fig. S16. Growth properties of Δ*acrB* and reference strain exposed to tetracycline.

(A) Difference in growth between M and D1 cells in a Δ*acrB* strain expressing cytoplasmic mCherry. Average and standard error of difference in growth ((M-D1)/M) between sister M and D1 cells is plotted in green for a and in purple for T. Data is pooled from 3 experiments, number of cells per interval: I-401; II-444; III-206; IV-111; V-46. Error bars=+/-1 SE. The difference in T is also shown in the main text Figure 3D.
(B) Difference in growth between M and D1 cells in a reference strain expressing cytoplasmic mCherry only. For the reference strain, changes in growth are qualitatively similar to the data shown in Figure 3 (see main text). Average and standard error of difference in growth ((M-D1)/M) between sister M and D1 cells is plotted in green for α and in purple for T. Data for (B) is pooled over 3 experiments, number of cells per interval: I-130; II-197; III-146; IV-108; V-81. Note that the IC50 of the Δ*acrB* strain is below the concentration at which M and D1 growth differences in the reference strain emerge. Thus, T and α cannot be determined in the Δ*acrB* strain above the IC50 due to strong filamentation.

Fig. S17.

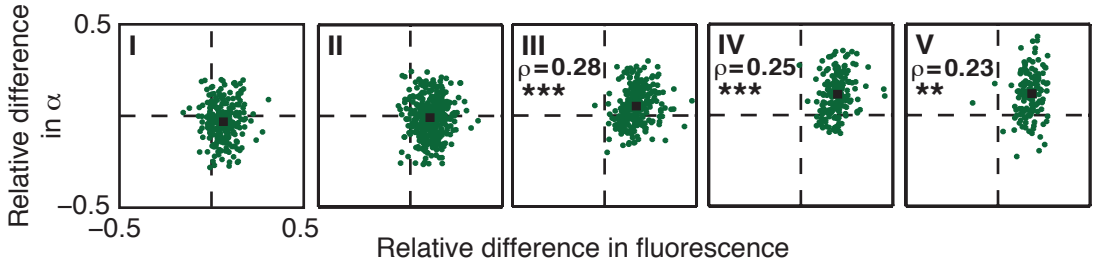

Fig. S17. Correlations between AcrB-GFP and elongation rate in the presence of fixed concentrations of tetracycline.

At higher antibiotic concentrations (III-V), differences in individual M-D1 pairs in AcrB-GFP expression correlate with differences in elongation rate ($\Delta\alpha$); r - Spearman correlation (**: $p<10^{-2}$; ***: $p<10^{-3}$). Data is pooled over three replicates of Tetracycline step-wise experiment, with sample sizes reported in SI Table S3.

Fig. S18.

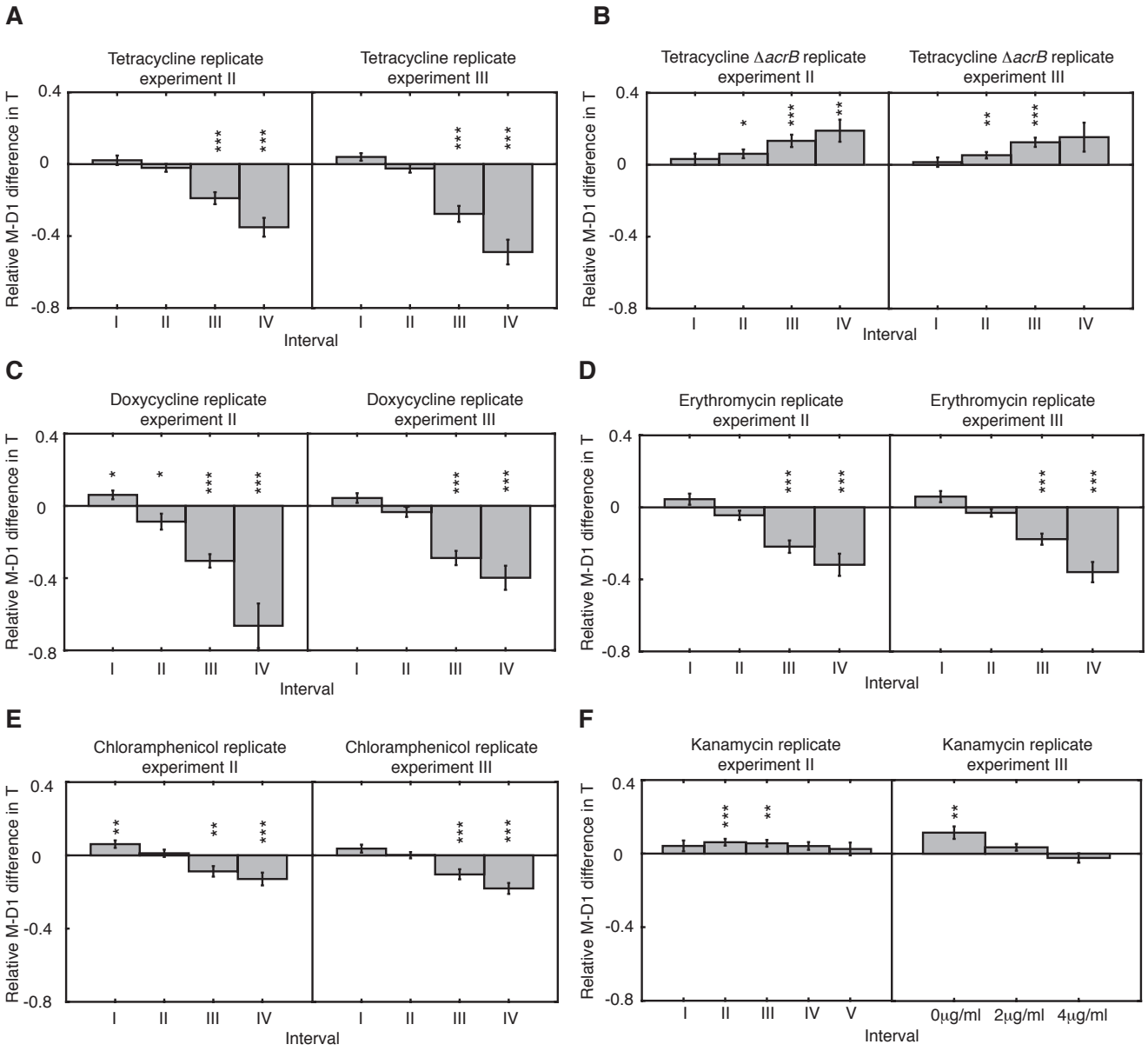
A
Tetracycline replicate experiment II
Tetracycline replicate experiment III
B
Tetracycline ΔacrB replicate experiment II
Tetracycline ΔacrB replicate experiment III
C
Doxycycline replicate experiment II
Doxycycline replicate experiment III
D
Erythromycin replicate experiment II
Erythromycin replicate experiment III
E
Chloramphenicol replicate experiment II
Chloramphenicol replicate experiment III
F
Kanamycin replicate experiment II
Kanamycin replicate experiment III
Relative M-D1 difference in T
Interval
I
II
III
IV
V
0μg/ml
2μg/ml
4μg/ml

Fig. S18. Replicate antibiotic exposure experiments

Relative differences in cell cycle duration (ΔT=(M-D1)/M) for sister M and D1 cells measured in two independent step-wise exposure experiments to the different antibiotics. Sample sizes are reported in Table S3. Significance is indicated by stars: * $p<0.05$, ** $p<0.01$, *** $p<0.001$. All cells carry an AcrB-GFP fusion except panel B (Δ*acrB* mutant) and panel F experiment III (both reference strain and AcrB-GFP fusion strain). (A) tetracycline, (B) tetracycline in Δ*acrB* strain, (C) doxycycline, (D) erythromycin, (E) chloramphenicol, (F) kanamycin. For the right panel of kanamycin we used slightly higher concentrations due to the nature of the antibiotic. We found that all antibiotics used in our study, with the exception of kanamycin, lead to strong filamentation when antibiotic concentrations approached the IC50 of the respective drug. Filamentation was particularly strong in mutants devoid of efflux by deletion of *acrB*, which prohibited reliable measurements of elongation rates and cell cycle duration at antibiotic concentrations approximating and exceeding IC50. While all antibiotics we used induced gradual changes in α and T, the response to kanamycin exhibited a sharp threshold at around 5μg/ml, at which cell growth bifurcated: cells either stopped dividing or continued to grow, albeit with reduced α and T. Bifurcation of cell growth after the addition of kanamycin was described previously (*37*), and is thought to stem from irreversible binding of kanamycin to the ribosome.

Fig. S19.

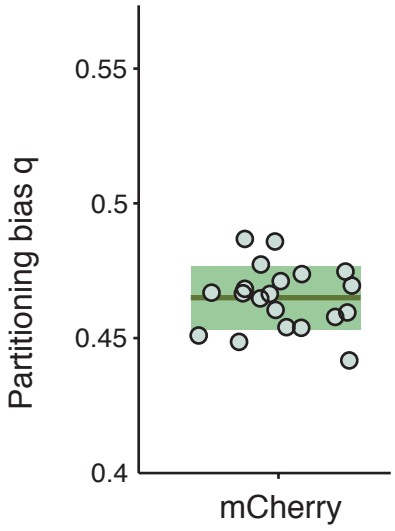

Fig. S19. Partitioning bias of cytosolic mCherry.

Bias q for individual lineages (dots) for partitioning of cytosolic mCherry in AcrB-GFP strain; Line and envelope = mean +/- STD over lineages.

Table S1.

(A)

Experiment 1	α	StDev	T	StDev	N	Divide
M	0.022	0.0028	34	9.1	714	97%
D1	0.023	0.0034	32	8.9	691	97%
D2	0.022	0.0038	32	8.6	671	83%
D3	0.022	0.0044	31	7.9	665	30%
Experiment 2	α	StDev	T	StDev	N	Divide
M	0.021	0.0026	36	11.4	484	96%
D1	0.022	0.0025	35	9.1	507	95%
D2	0.021	0.0032	36	8.8	475	70%
D3	0.021	0.0037	32	7.5	483	7%

(B)

	α	StDev	T	StDev	N	Divide
M	0.020	0.0020	37	8.6	643	96%
D1	0.021	0.0020	34	8.8	605	95%
D2	0.021	0.0026	35	8.2	568	66%
D3	0.020	0.0028	31	8.5	567	6%

Table S1. Growth stability in microfluidic devices

(A) Summary of average growth rates for cells expressing AcrB-GFP and cytoplasmic mCherry. Experiment 1 comprises data from 20 colonies data used in Figure 4. Experiment 2 comprises data from 22 colonies data used in Figure 1D and 1E.
(B) Summary of average growth rates for cells expressing cytoplasmic mCherry only. Data from 28 colonies.

Table S2.

Experiment 1	Asymmetry	p value
M	0.34	$2x10^{-7}$
D1	0.02	10^{-7}
D2	0.05	10^{-39}
D3	0.10	10^{-92}
Experiment 2	Asymmetry	p value
M	0.42	$2x10^{-5}$
D1	0.03	10^{-8}
D2	0.05	10^{-29}
D3	0.11	10^{-97}
Experiment 3	Asymmetry	p value
M	0.27	10^{-11}
D1	0.06	10^{-25}
D2	0.07	10^{-43}
D3	0.12	10^{-102}

Table S2. AcrB-GFP accumulates at old cell poles.

Old and new cell halves differ significantly in AcrB-GFP fluorescence, with the asymmetry correlated to older pole age. Asymmetry defined as in Figure 1D of the main text, significance assessed by t-test. In cells carrying a pole of age 2 (D3 daughter cells), this difference is approximately 10%. Since each microfluidic channel contains one mother (M) cell only, which gives rise to multiple daughter (D) cells, the sample size and thus significance for M cells is smaller.

Table S3.

Elongation rate α	Interval				
AcrB-GFP	I	II	III	IV	V
Exp 1	-0.04 (**)	-0.03 (*)	0.06 (***)	0.08 (**)	0.03 (ns)
Exp 2	-0.06 (***)	-0.01 (ns)	0.02 (ns)	0.10(***)	0.11 (***)
Exp 3	-0.01 (ns)	0.00 (ns)	0.06 (***)	0.15 (***)	0.16 (***)
No protein fusion					
Exp 1	-0.01 (ns)	-0.13 (ns)	0.09 (***)	0.11 (***)	0.07 (ns)
Exp 2	-0.01 (ns)	-0.25 (ns)	0.11 (***)	0.19 (***)	0.16 (***)
Exp 3	-0.03 (*)	-0.02 (ns)	0.05 (***)	0.16 (***)	0.21 (***)

Cell cycle duration T	Interval				
AcrB-GFP	I	II	III	IV	V
Exp 1	-0.01 (ns)	-0.04 (ns)	-0.38 (***)	-0.29 (***)	-0.14 (ns)
Exp 2	0.02 (ns)	-0.02 (ns)	-0.19 (***)	-0.35 (***)	-0.39 (***)
Exp 3	0.04 (ns)	-0.02 (ns)	-0.28 (***)	-0.49 (***)	-0.34 (***)
No protein fusion					
Exp 1	-0.03 (ns)	-0.04 (ns)	-0.44 (***)	-0.52 (**)	-0.30 (ns)
Exp 2	0.03 (ns)	0.05 (ns)	-0.28 (***)	-0.58 (***)	-0.31 (**)
Exp 3	0.05 (*)	-0.01 (ns)	-0.26 (***)	-0.58 (***)	-0.46 (***)

Number of cells	Interval				
AcrB-GFP	I	II	III	IV	V
Exp 1	73	116	71	47	31
Exp 2	87	185	129	94	71
Exp 3	100	129	88	60	43
No protein fusion					
Exp 1	23	33	23	17	14
Exp 2	27	66	49	35	26
Exp 3	80	98	74	56	41

Table S3. Overview of replicate tetracycline exposure experiments

Growth measured by elongation rate α and cell cycle duration T. Reported value is the mean relative difference of the sister cells $(\alpha_M-\alpha_{D1})/\alpha_M$ (top) and $(T_M-T_{D1})/T_M$ (middle) per interval for each of the three repeat experiments. P-values from t-test to determine whether the relative difference is non-zero. Significance is indicated by stars, * $p<0.05$, ** $p<0.01$, *** $p<0.001$. The number of M-D1 pairs at the end of the interval per experiment is reported on the bottom third of the table. In experiment 1 interval I lasts for 156 min, experiment 2 interval I for 120min, experiment 3 interval I for 234min. All subsequent intervals have the same duration in all experiments and last for 300min. Tetracycline concentration per interval: I-0μg/ml; lI-0.1875μg/ml; III-0.375μg/ml; IV-0.6525μg/ml; V-0.75μg/ml. Statistical note: the pattern of statistical significance remains nearly unchanged if we use a two-sided t-test to determine whether elongation rates and cell division times are drawn from distributions with equal means for M and D1 cells in different intervals / repeat experiments.

Table S4.

Number of cells	Interval				
Antibiotic	I	II	III	IV	V
Doxycycline 1	100	109	99	73	53
Doxycycline 2	132	204	130	100	78
Doxycycline 3	103	142	98	65	46
Tetracycline Δ*acrB* 1	58	87	47	21	17
Tetracycline Δ*acrB* 2	128	145	67	35	16
Tetracycline Δ*acrB* 3	185	212	102	55	13
Erythromycin 1	84	102	90	64	23
Erythromycin 2	86	139	105	55	22
Erythromycin 3	95	157	110	66	24
Chloramphenicol 1	159	187	121	68	38
Chloramphenicol 2	138	194	137	91	67
Chloramphenicol 3	157	211	157	128	65
Kanamycin 1	92	118	113	98	30
Kanamycin 2	112	161	153	144	65
Kanamycin 3	61	204	152	13	0

Table S4. Number of M-D1 pairs per experiment in the main text Figure 3D

Number of M-D1 pairs per experiment in the main text Figure 3D. Kanamycin 3 intervals correspond to different concentrations of kanamycin than kanamycin 1 and 2. See Table S5 for details.

Table S5.

Antibiotic concentration μg/ml	Interval				
Antibiotic	I	II	III	IV	V
Doxycycline	0	0.1875	0.375	0.5625	0.75
Chloramphenicol	0	1	2	3	4
Erythromycin	0	6.25	12.5	18.75	25
Kanamycin 1 and 2	0	1.25	2.5	3.75	5
Kanamycin 3	0	2	4	6	8
Tetracycline Δ*acrB* strain	0	0.0625	0.125	0.1875	0.25

Table S5. Antibiotic concentrations used in experiments shown in Figure 3D

Antibiotic concentrations (μg/ml) used in experiments shown in Figure 3D. The concentrations were tuned so that interval V corresponds to approximately IC50, except for experiment Kanamycin 3.

Table S6.

Antibiotic	Class	Target	Mode of action
Tetracycline	Tetracyclines	30s ribosomal subunit	Inhibition of amino-acyl-tRNA binding
Doxycycline	Tetracyclines	30s ribosomal subunit	Inhibition of amino-acyl-tRNA binding
Kanamycin	Aminoglycosides	30s ribosomal subunit	Causes mistranslation
Chloramphenicol	Amphenicols	50s ribosomal subunit	Prevention of protein chain elongation
Erythromycin	Macrolides	50s ribosomal subunit	Prevention of protein chain elongation

Table S6. Antibiotics used in this study

Table S7.

	Interval				
Antibiotic	T_I	T_{II}/T_I	T_{III}/T_I	T_{IV}/T_I	T_V/T_I
Tetracycline 1	33.5 min	1.32 (***)	2.16 (***)	3.48 (***)	-
Tetracycline 2	31.7 min	1.30 (***)	1.86 (***)	2.54 (***)	-
Tetracycline 3	36.6 min	1.15 (***)	1.64 (***)	2.17 (***)	-
Doxycycline 1	33.7 min	1.30 (***)	2.04 (***)	2.90 (***)	-
Doxycycline 2	36.4 min	1.40 (***)	1.93 (***)	2.51 (***)	-
Doxycycline 3	36.1 min	1.50 (***)	2.14 (***)	3.16 (***)	-
Tetracycline Δ*acrB* 1	34.5 min	1.28 (***)	2.69 (***)	5.38 (***)	-
Tetracycline Δ*acrB* 2	35.9 min	1.36 (***)	2.70 (***)	4.47 (***)	-
Tetracycline Δ*acrB* 3	35.4 min	1.35 (***)	2.61 (***)	4.75 (***)	-
Erythromycin 1	34.9 min	1.22 (***)	1.75 (***)	2.67 (***)	-
Erythromycin 2	32.3 min	1.31 (***)	1.74 (***)	2.42 (***)	-
Erythromycin 3	32.5 min	1.30 (***)	1.91 (***)	2.50 (***)	-
Chloramphenicol 1	35.2 min	1.10 (**)	1.69 (***)	2.46 (***)	-
Chloramphenicol 2	37.4 min	1.12 (***)	1.58 (***)	2.07 (***)	-
Chloramphenicol 3	34.7 min	1.17 (***)	1.60 (***)	1.97 (***)	-
Kanamycin 1	35.3 min	1.01 (ns)	1.06 (ns)	1.53 (***)	-
Kanamycin 2	35.5 min	1.08 (*)	1.11 (**)	1.19 (***)	1.63 (***)
Kanamycin 3	34.3 min	1.08 (ns)	1.89 (***)	-	-

Table S7. Cell cycle duration in interval I and relative cell cycle duration in intervals II-V

Mean cell cycle duration, T, of M cells in interval I and relative increase in T in M cells in intervals II-V per experiment in the main text Figure 3D and Figure S18. P-values from t-test to determine whether mean T is different in different intervals. Significance is indicated by stars, * $p<0.05$, ** $p<0.01$, *** $p<0.001$. Kanamycin 3 intervals correspond to different concentrations of kanamycin than kanamycin 1 and 2. See Table S5 for details. Kanamycin 3 data combines wt strain and strain with AcrB-GFP. All other experiments were carried out with AcrB-GFP strain.

Table S8.

Erythromycin µg/ml	**MG1655**	**Δ*acrB***	**Δ*tolC***
100	0.621+/-0.001	0.058+/-0.003	0.016+/-0.001
50	0.793+/-0.002	0.116+/-0.006	0.018+/-0.001
25	0.871+/-0.002	0.224+/-0.004	0.020+/-0.001
12.5	0.914+/-0.003	0.439+/-0.025	0.021+/-0.001
6.25	0.950+/-0.004	0.769+/-0.014	0.030+/-0.001
3.125	0.975+/-0.009	0.895+/-0.022	0.089+/-0.001
Doxycycline µg/ml	**MG1655**	**Δ*acrB***	**Δ*tolC***
5	0.004+/-0.000	0.010+/-0.000	0.016+/-0.000
2.5	0.009+/-0.005	0.012+/-0.000	0.014+/-0.000
1.25	0.713+/-0.028	0.026+/-0.000	0.025+/-0.000
0.625	0.850+/-0.005	0.088+/-0.020	0.057+/-0.003
0.3125	0.894+/-0.011	0.188+/-0.004	0.101+/-0.002
Chloramphenicol µg/ml	**MG1655**	**Δ*acrB***	**Δ*tolC***
5	0.166+/-0.010	0.018+/-0.000	0.018+/-0.003
2.5	0.776+/-0.004	0.027+/-0.000	0.025+/-0.004
1.25	0.826+/-0.007	0.187+/-0.026	0.122+/-0.015
0.625	0.978+/-0.015	0.859+/-0.008	0.897+/-0.111
0.3125	0.978+/-0.010	0.882+/-0.028	0.935+/-0.121
Kanamycin µg/ml	**MG1655**	**Δ*acrB***	**Δ*tolC***
25	0.170+/-0.094	0.189+/-0.012	0.056+/-0.003
12.5	0.103+/-0.008	0.064+/-0.007	0.148+/-0.004
6.25	0.512+/-0.012	0.268+/-0.020	0.471+/-0.011
3.125	0.904+/-0.013	0.816+/-0.026	0.908+/-0.015
1.5625	1.052+/-0.023	0.989+/-0.024	1.002+/-0.023

Table S8. Serial dilutions of reference, Δ*acrB* and Δ*tolC* strains in antibiotics used for Figure 3D

Values report on $OD600_{nm}$ relative to the untreated control. Indicated error is one STE.

Table S9. Strains

MG1655	*rph-1* LAM-	Lab strain collection
BW27784	F- Δ(*araD*-araB)*567* Δ*lacZ4787*(::*rrnB-3*) λ^- Δ (*araH*-araF 570::*FRT*) Δ*araEp-532*::*FRT* ϕP_{cp18}*araE533* Δ(*rhaD-rhaB*)*568 hsdR514*	(*31*)
DH5α	F^- *endA1 glnV44 thi-1 recA1 relA1 gyrA96 deoR nupG purB20* ϕ*80dlacZ*Δ*M15* Δ(*lacZYA-argF*)*U169*, *hsdR17*($r_K^- m_K^+$), λ^-	Lab strain collection
DH5α λpir	F^- *endA1 glnV44 thi-1 recA1 relA1 gyrA96 deoR nupG purB20* ϕ*80dlacZ*Δ*M15* Δ(*lacZYA-argF*)*U169*, *hsdR17*($r_K^- m_K^+$), λpir+	Lab strain collection
DY330	W3110 *lacU169 gal490 (*λ*cI857* Δ*(cro-bioA))*	(*27*)
JW0451	Δ*acrB::kan donor*	(*34*)
JW5503	Δ*tolC::kan donor*	(*34*)
TB203	*acrB-gfp*::*FRT* Δ*fliC*::*FRT attP21*::PR-*mCherry*::*FRT*	This work
TB205	*attP21*::PR-*mCherry*::*FRT* Δ*fliC*::*FRT*	This work
TB222	*acrB-mVenus*::*FRT* Δ*fliC*::*FRT attP21*::PR-*mCherry*::*FRT*	This work
TB271	*attP21*::*PR-mCherry*::*frt* Δ*acrB*::*FRT*	This work
TB283	*attP21*::*PR-mCherry*::*frt* Δ*tolC*::*FRT*	This work
TB360	*acrB-gfp*::*FRT* Δ*fliC*::*FRT attP21*::PR-*mCherry*::*FRT* Δ*tolC*::*FRT*	This work
TB356	*acrB-gfp*::*FRT* Δ*fliC*::*FRT attP21*::PR-*mCherry*::*FRT* Δ*tolC*::*FRT att*λ*::pAH55-tolC(*P_{tac}*-tolC)-neo(kan)*	This work
TB275	BW27784 *attP21*::*PR-mCherry*::*frt* Δ*acrR FRT*::*araC*-P_{araBAD}*-acrAB-gfp::FRT*	This work
TB276	BW27784 *attP21*::*PR-mCherry*::*frt* Δ*acrR FRT*::*araC*-P_{araBAD}*-acrAB*	This work
TB224	*acrB-3xFlag*::*FRT* Δ*fliC*::*FRT attP21*::*PR-mCherry*::*chlor*	This work
TB342	*tolC-gfp*::*chlor*	This work
TB345	*attP21*::*PR-mCherry*::*frt* Δ*fliC*::*FRT tolC-gfp*::*FRT*	This work
TB370	*attP21*::*PR-mCherry*::*frt* Δ*fliC*::*FRT tolC-gfp*::*FRT* Δ*acrAB*::*kan*	This work
TB371	*tolC-gfp*::*FRT* Δ*acrAB*::*kan*	This work

Table S10.

GAATGAAGATATCGAGCACAGCCATACTGTCGAT CATCATggtagcggtaacaaaggtcagggcagcaagggcgaggagctgtt	5_acrB-gfp-insert
ATGTTCGTAGGTTATGCATAAAAAAGGCCGCTTA CGCGGCattagccatggtccatatga	3_acrB-gfp-insert
ACGCACTACCACCAGTAACGGTCATAACCCTTTCC GTAACggtagcggtaacaaaggtcagggcAGCAAGGGCGAGG AGCTGTT	5_tolC-gfp-insert
GATAACCCGTATCTTTACGTTGCCTTACGTTCAGA CGGGGattagccatggtccatatga	3_tolC-gfp-insert
ACGAAAATGTCCAGGAAAAATCCTGGAGTCAGAT TCAGGGaatgtgcctgtcaaatggacg	5_ParaBAD-swap-acrAB
GTCAAAAGTTAATAAACCCATTGCTGCGTTTATAT TATCGTatggagaaacagtagagagt	3_ParaBAD-swap-acrAB
GAATGAAGATATCGAGCACAGCCATACTGTCGAT CATCATGactacaaagaccatgacgg	5_acrB-3xFlag-insert
CTTAATGTTCGTAGGTTATGCATAAAAAAGGCCG CTTACGTatgaatatcctccttag	3_acrB-3xFlag-insert

Table S10. Oligonucleotides

Upper case sequences highlight homologies to the *E. coli* MG1655 chromosome.

Table S11. Replication of experiments

A) Experiments for main figures

Figure 1	
Panels B to D, efflux pump polar localization and accumulation.	- AcrB-GFP: three independent repeats - AcrB-GFP in Δ*tolC* strain background: two independent experiments - AcrB-mVenus: one experiment A subset of these repeats is shown in Figure S5
Panel F	Taken from the experiment shown in Figure 1 panel D
Panel G, pulse-chase experiment	Three independent repeats, kymographs of two replicates shown in Figure S7
Figure 2	
Panels A and B, single-cell efflux activity	- Two independent repeats with Δ*tolC* strain - Three independent repeats with each strain
Figure 3	
All panels	All experiments with stepwise increasing antibiotic concentrations have been repeated three times, all replicate experiments are shown in Figure S18

B) Supplementary figures

Figure S2	
MIC measurements	- Two independent experiments, one is shown in Figure S2
Figure S4	
Robust growth	- Data taken from the experiment shown in Figure 1D and E, which has been replicated as indicated
Figure S6	
Antibody staining of AcrB-3xFlag	- Two independent replicates
Figure S7	
TolC induction	- Panel A: MICs were measured once - Panel C: Each IPTG concentration was measured once - Panel D: Promoter activity was replicated twice independently
Figure S9	
TolC-GFP localization and accumulation	The experiment was replicated twice independently, one replicate shown
Figure S10	
Pulse-chase of AcrB-GFP	- The experiment was replicated twice independently, kymographs of two replicates shown in this SI Figure - MIC measurements were performed once
Figure S11	
Cluster segregation	Two independent experiments were performed with each strain
Figure S12	
Single-cell efflux	In total three independent repeats per strain with and without AcrB-GFP fusion
Figure S13	
FACS-sorting experiments	The experiment was repeated twice independently as shown in the SI Figure
SI Figure 15	
Single exposure to tetracycline	The experiment was replicated independently twice
SI Figure 16 and 17	
Growth properties after exposure to tetracycline	Three independent repeats of each experiment were conducted

Movie S1: Polar accumulation of AcrB-GFP

AcrB-GFP accumulates at the old mother cell pole over time, and accumulation is TolC-dependent. Images were recorded every 6min, and compressed into 10 frames/s. Left: mCherry, right: AcrB-GFP. Left channel: AcrB-GFP Δ*tolC*; right channel: AcrB-GFP. Scale bar: 2μm.

Movie S2: Pulse-chase of P_{araBAD}-*acrB-gfp* and P_{araBAD}-*gfp*

P_{araBAD}-*acrB-gfp* and P_{araBAD}-*gfp* expression was induced with 0.05% L-arabinose after 120 min, and L-arabinose was washed out after 360min. Images were recorded every 4min, and compressed into 10 frames/s. Left: mCherry, right: AcrB-GFP and GFP. Scale bar: 2μm.

Movie S3: Exposure to increasing concentrations of tetracycline

AcrB-GFP-expressing cells were exposed to increasing tetracycline concentrations (see main text). Period I (no drug) 0min to 240min; each following tetracycline interval II to V lasts 300min. Images were recorded every 6min, and compressed into 10 frames/s. Left: mCherry, right: AcrB-GFP and GFP. Scale bar: 2μm.

References

1. A. Sanchez, S. Choubey, J. Kondev, Regulation of noise in gene expression. *Annu. Rev. Biophys.* **42**, 469–491 (2013). doi:10.1146/annurev-biophys-083012-130401 Medline

2. N. A. Cookson, W. H. Mather, T. Danino, O. Mondragón-Palomino, R. J. Williams, L. S. Tsimring, J. Hasty, Queueing up for enzymatic processing: Correlated signaling through coupled degradation. *Mol. Syst. Biol.* **7**, 561 (2011). doi:10.1038/msb.2011.94 Medline

3. D. Huh, J. Paulsson, Random partitioning of molecules at cell division. *Proc. Natl. Acad. Sci. U.S.A.* **108**, 15004–15009 (2011). doi:10.1073/pnas.1013171108 Medline

4. M. A. de Pedro, C. G. Grünfelder, H. Schwarz, Restricted mobility of cell surface proteins in the polar regions of *Escherichia coli*. *J. Bacteriol.* **186**, 2594–2602 (2004). doi:10.1128/JB.186.9.2594-2602.2004 Medline

5. P. Rassam, N. A. Copeland, O. Birkholz, C. Tóth, M. Chavent, A. L. Duncan, S. J. Cross, N. G. Housden, R. Kaminska, U. Seger, D. M. Quinn, T. J. Garrod, M. S. P. Sansom, J. Piehler, C. G. Baumann, C. Kleanthous, Supramolecular assemblies underpin turnover of outer membrane proteins in bacteria. *Nature* **523**, 333–336 (2015). doi:10.1038/nature14461 Medline

6. C. Kleanthous, P. Rassam, C. G. Baumann, Protein-protein interactions and the spatiotemporal dynamics of bacterial outer membrane proteins. *Curr. Opin. Struct. Biol.* **35**, 109–115 (2015). doi:10.1016/j.sbi.2015.10.007 Medline

7. J. Dworkin, Cellular polarity in prokaryotic organisms. *Cold Spring Harb. Perspect. Biol.* **1**, a003368 (2009). doi:10.1101/cshperspect.a003368 Medline

8. T. J. Silhavy, D. Kahne, S. Walker, The bacterial cell envelope. *Cold Spring Harb. Perspect. Biol.* **2**, a000414–a000414 (2010). doi:10.1101/cshperspect.a000414 Medline

9. X.-Z. Li, P. Plésiat, H. Nikaido, The challenge of efflux-mediated antibiotic resistance in Gram-negative bacteria. *Clin. Microbiol. Rev.* **28**, 337–418 (2015). doi:10.1128/CMR.00117-14 Medline

10. D. Du, Z. Wang, N. R. James, J. E. Voss, E. Klimont, T. Ohene-Agyei, H. Venter, W. Chiu, B. F. Luisi, Structure of the AcrAB-TolC multidrug efflux pump. *Nature* **509**, 512–515 (2014). doi:10.1038/nature13205 Medline

11. Materials and methods are available as supplementary materials.

12. H. I. Zgurskaya, G. Krishnamoorthy, A. Ntreh, S. Lu, Mechanism and function of the outer membrane channel TolC in multidrug resistance and physiology of enterobacteria. *Front. Microbiol.* **2**, 189 (2011). doi:10.3389/fmicb.2011.00189 Medline

13. M. C. Sulavik, C. Houseweart, C. Cramer, N. Jiwani, N. Murgolo, J. Greene, B. DiDomenico, K. J. Shaw, G. H. Miller, R. Hare, G. Shimer, Antibiotic susceptibility profiles of *Escherichia coli* strains lacking multidrug efflux pump genes. *Antimicrob. Agents Chemother.* **45**, 1126–1136 (2001). doi:10.1128/AAC.45.4.1126-1136.2001 Medline

14. K. Nishino, A. Yamaguchi, Analysis of a complete library of putative drug transporter genes in *Escherichia coli*. *J. Bacteriol.* **183**, 5803–5812 (2001). doi:10.1128/JB.183.20.5803-5812.2001 Medline

15. P. Wang, L. Robert, J. Pelletier, W. L. Dang, F. Taddei, A. Wright, S. Jun, Robust growth of *Escherichia coli*. *Curr. Biol.* **20**, 1099–1103 (2010). doi:10.1016/j.cub.2010.04.045 Medline

16. J. L. Rosner, R. G. Martin, An excretory function for the *Escherichia coli* outer membrane pore TolC: Upregulation of marA and soxS transcription and Rob activity due to metabolites accumulated in tolC mutants. *J. Bacteriol.* **191**, 5283–5292 (2009). doi:10.1128/JB.00507-09 Medline

17. N. G. Coldham, M. Webber, M. J. Woodward, L. J. V. Piddock, A 96-well plate fluorescence assay for assessment of cellular permeability and active efflux in *Salmonella enterica* serovar Typhimurium and *Escherichia coli*. *J. Antimicrob. Chemother.* **65**, 1655–1663 (2010). doi:10.1093/jac/dkq169 Medline

18. E. Gullberg, S. Cao, O. G. Berg, C. Ilbäck, L. Sandegren, D. Hughes, D. I. Andersson, Selection of resistant bacteria at very low antibiotic concentrations. *PLOS Pathog.* **7**, e1002158 (2011). doi:10.1371/journal.ppat.1002158 Medline

19. B. M. C. Martins, J. C. Locke, Microbial individuality: How single-cell heterogeneity enables population level strategies. *Curr. Opin. Microbiol.* **24**, 104–112 (2015). doi:10.1016/j.mib.2015.01.003 Medline

20. T. M. Norman, N. D. Lord, J. Paulsson, R. Losick, Stochastic Switching of Cell Fate in Microbes. *Annu. Rev. Microbiol.* **69**, 381–403 (2015). doi:10.1146/annurev-micro-091213-112852 Medline

21. S. Leibler, E. Kussell, Individual histories and selection in heterogeneous populations. *Proc. Natl. Acad. Sci. U.S.A.* **107**, 13183–13188 (2010). doi:10.1073/pnas.0912538107 Medline

22. D. I. Andersson, D. Hughes, Gene amplification and adaptive evolution in bacteria. *Annu. Rev. Genet.* **43**, 167–195 (2009). doi:10.1146/annurev-genet-102108-134805 Medline

23. F. Baquero, J. L. Martínez, R. Cantón, Antibiotics and antibiotic resistance in water environments. *Curr. Opin. Biotechnol.* **19**, 260–265 (2008). doi:10.1016/j.copbio.2008.05.006 Medline

24. F. Baquero, M. C. Negri, Selective compartments for resistant microorganisms in antibiotic gradients. *BioEssays* **19**, 731–736 (1997). doi:10.1002/bies.950190814 Medline

25. D. Laehnemann, R. Peña-Miller, P. Rosenstiel, R. Beardmore, G. Jansen, H. Schulenburg, Genomics of rapid adaptation to antibiotics: Convergent evolution and scalable sequence amplification. *Genome Biol. Evol.* **6**, 1287–1301 (2014). doi:10.1093/gbe/evu106 Medline

26. O. Mondragón-Palomino, T. Danino, J. Selimkhanov, L. Tsimring, J. Hasty, Entrainment of a population of synthetic genetic oscillators. *Science* **333**, 1315–1319 (2011). doi:10.1126/science.1205369 Medline

27. D. Yu, H. M. Ellis, E.-C. Lee, N. A. Jenkins, N. G. Copeland, D. L. Court, An efficient recombination system for chromosome engineering in *Escherichia coli*. *Proc. Natl. Acad. Sci. U.S.A.* **97**, 5978–5983 (2000). doi:10.1073/pnas.100127597 Medline

28. A. Haldimann, B. L. Wanner, Conditional-replication, integration, excision, and retrieval plasmid-host systems for gene structure-function studies of bacteria. *J. Bacteriol.* **183**, 6384–6393 (2001). doi:10.1128/JB.183.21.6384-6393.2001 Medline

29. K. A. Datsenko, B. L. Wanner, One-step inactivation of chromosomal genes in *Escherichia coli* K-12 using PCR products. *Proc. Natl. Acad. Sci. U.S.A.* **97**, 6640–6645 (2000). doi:10.1073/pnas.120163297 Medline

30. T. Bergmiller, M. Ackermann, O. K. Silander, Patterns of evolutionary conservation of essential genes correlate with their compensability. *PLOS Genet.* **8**, e1002803 (2012). doi:10.1371/journal.pgen.1002803 Medline

31. A. Khlebnikov, K. A. Datsenko, T. Skaug, B. L. Wanner, J. D. Keasling, Homogeneous expression of the P(BAD) promoter in *Escherichia coli* by constitutive expression of the low-affinity high-capacity AraE transporter. *Microbiology* **147**, 3241–3247 (2001). doi:10.1099/00221287-147-12-3241 Medline

32. A. Zaslaver, A. Bren, M. Ronen, S. Itzkovitz, I. Kikoin, S. Shavit, W. Liebermeister, M. G. Surette, U. Alon, A comprehensive library of fluorescent transcriptional reporters for *Escherichia coli*. *Nat. Methods* **3**, 623–628 (2006). doi:10.1038/nmeth895 Medline

33. D. Landgraf, B. Okumus, P. Chien, T. A. Baker, J. Paulsson, Segregation of molecules at cell division reveals native protein localization. *Nat. Methods* **9**, 480–482 (2012). doi:10.1038/nmeth.1955 Medline

34. T. Baba, T. Ara, M. Hasegawa, Y. Takai, Y. Okumura, M. Baba, K. A. Datsenko, M. Tomita, B. L. Wanner, H. Mori, Construction of *Escherichia coli* K-12 in-frame, single-gene knockout mutants: The Keio collection. *Mol. Syst. Biol.* **2**, 0008 (2006). doi:10.1038/msb4100050 Medline

35. K. Yamamoto, R. Tamai, M. Yamazaki, T. Inaba, Y. Sowa, I. Kawagishi, Substrate-dependent dynamics of the multidrug efflux transporter AcrB of *Escherichia coli*. *Sci. Rep.* **6**, 21909 (2016). doi:10.1038/srep21909 Medline

36. T. S. Ursell, J. Nguyen, R. D. Monds, A. Colavin, G. Billings, N. Ouzounov, Z. Gitai, J. W. Shaevitz, K. C. Huang, Rod-like bacterial shape is maintained by feedback between cell curvature and cytoskeletal localization. *Proc. Natl. Acad. Sci. U.S.A.* **111**, E1025–E1034 (2014). doi:10.1073/pnas.1317174111 Medline

37. P. Greulich, M. Scott, M. R. Evans, R. J. Allen, Growth-dependent bacterial susceptibility to ribosome-targeting antibiotics. *Mol. Syst. Biol.* **11**, 796 (2015). doi:10.15252/msb.20145949 Medline